

Review

# In Vivo Assessment of Synthetic and Biological-Derived Calcium Phosphate-Based Coatings Fabricated by Pulsed Laser Deposition: A Review

Liviu Duta 

Lasers Department, National Institute for Lasers, Plasma and Radiation Physics, 409 Atomistilor Street, 077125 Magurele, Romania; liviu.duta@inflpr.ro; Tel.: +40-21-457-4550 (ext. 2023)

**Abstract:** The aim of this review is to present the state-of-the-art achievements reported in the last two decades in the field of pulsed laser deposition (PLD) of biocompatible calcium phosphate (CaP)-based coatings for medical implants, with an emphasis on their *in vivo* biological performances. There are studies in the dedicated literature on the *in vivo* testing of CaP-based coatings (especially hydroxyapatite, HA) synthesized by many physical vapor deposition methods, but only a few of them addressed the PLD technique. Therefore, a brief description of the PLD technique, along with some information on the currently used substrates for the synthesis of CaP-based structures, and a short presentation of the advantages of using various animal and human implant models will be provided. For an in-depth *in vivo* assessment of both synthetic and biological-derived CaP-based PLD coatings, a special attention will be dedicated to the results obtained by standardized and micro-radiographies, (micro) computed tomography and histomorphometry, tomodensitometry, histology, scanning and transmission electron microscopies, and mechanical testing. One main specific result of the *in vivo* analyzed studies is related to the demonstrated superior osseointegration characteristics of the metallic (generally Ti) implants functionalized with CaP-based coatings when compared to simple (control) Ti ones, which are considered as the “gold standard” for implantological applications. Thus, all such important *in vivo* outcomes were gathered, compiled and thoroughly discussed both to clearly understand the current status of this research domain, and to be able to advance perspectives of these synthetic and biological-derived CaP coatings for future clinical applications.

**Keywords:** calcium phosphate-based coatings; synthetic and natural hydroxyapatite; pulsed laser deposition; *in vivo* testing; biomedical applications



**Citation:** Duta, L. In Vivo Assessment of Synthetic and Biological-Derived Calcium Phosphate-Based Coatings Fabricated by Pulsed Laser Deposition: A Review. *Coatings* **2021**, *11*, 99. <https://doi.org/10.3390/coatings11010099>

Received: 11 December 2020

Accepted: 12 January 2021

Published: 18 January 2021

**Publisher's Note:** MDPI stays neutral with regard to jurisdictional claims in published maps and institutional affiliations.



**Copyright:** © 2021 by the author. Licensee MDPI, Basel, Switzerland. This article is an open access article distributed under the terms and conditions of the Creative Commons Attribution (CC BY) license (<https://creativecommons.org/licenses/by/4.0/>).

## 1. Introduction

The biomedical domain has witnessed over the last decades a significant development due to an extensive demand for a wide variety of implants, grafts, and/or scaffolds. The bone tissue engineering field has therefore expanded to be able to address a wide spectrum of bone-related injuries and offer viable and efficient solutions. This is mainly achieved by combining the properties of bioactive materials and cells for an improved and faster bone tissue ingrowth. Implants' surface functionalization and modification with performant bioactive materials is of high interest as it provides various possibilities to modify the surface properties of biomaterials to make them suitable for specific medical applications. This technology is currently applied both for the prevention of failure and the prolongation of the bone implants' life [1]. The fabrication of resistant implants able to bypass the difficulties related to their rejection from the living bodies is therefore of huge research interest. It is important to note that the global market for implantable medical devices was valued at \$72,265 million in 2015 and foreseen to attain \$116,300 million in 2022 [2].

Calcium phosphates (CaP) represent the main inorganic component of bone tissues [3]. They are the most utilized bioceramics in the medical field (i.e., orthopedics and

dentistry [4–7]), as coatings for a wide range of metallic implants [8]. In the last few decades, research emphasis was put on hydroxyapatite (HA), which is the most frequently used CaP due to some interesting characteristics, such as its role as scaffold for osteogenic differentiation [9] and its capacity to stimulate and accelerate new bone formation around implants [10–12]. One should note that there are currently two ways to obtain HA: the first one uses inorganic synthesis by different chemical routes (i.e., hydrothermal [13], co-precipitation [14], or sol–gel [15]). In the case of hydrothermal method, the synthesis temperature is relatively low, and the reaction conditions are moderate. The obtained products have high crystallinity, high purity, and controllable shape and size [16]. The chemical precipitation of nano-sized powders from salt solutions allows for the rapid synthesis of large amounts of material in a controlled manner [17]. The sol–gel process is a wet chemical method that involves atomic level molecular mixing, and provides good control over the composition and chemical homogeneity [18]. It should be emphasized that some of these approaches imply the use of complex processes, which could generate pollutant chemical wastes. Moreover, the composition of synthetic CaP is more complex than the one of biological-derived apatites due to both multiple lattice substitutions and the presence of ion vacancies [19]. As a consequence, a good alternative to classical chemical routes (i.e., extraction from renewable CaP resources) was introduced. One should note that the most important primary natural reservoirs of CaP are either bones (of mammalian [20,21] or fish [22,23] origin) or biogenic sources (egg-shells [24], mussel shells [25], or marine shells [26]). Unfortunately, these are generally treated as food industry wastes only [27]. Besides its low production cost, another great advantage of this fabrication route is the preservation of compositional and structural properties of the source material [28]. Furthermore, these as-fabricated biological-derived HA (BioHA) materials are well-suited to achieve a perfect synergy with the biological media due to their content in trace elements [4,8]. These elements have a determining role in the proper adjustment of biological properties (i.e., solubility, surface chemistry, and morphology), to keep compatible with the natural human bone [5,29]. As compared to chemically-synthesized HA, BioHA has different composition, stoichiometry, degree of crystallinity, degradation rate, and overall biological performance. From the biomimetic point of view, BioHA materials are more appropriate than synthetic HA to repair the skeletal system. It was reported that HA obtained from renewable, low-cost resources (i.e., animal or fish bones and egg-shells) can lead to physical-chemical characteristics and biological response comparable or even improved than those obtained in the case of synthetic ones, due to their resemblance with bone apatite [30,31]. The conversion of these by-products into HA is envisaged both as a strategy for wastes management and an economically feasible approach to reduce the overall costs for HA production. As compared to synthetic HA, the osseointegration speed of BioHA takes place more rapid due to its higher solubility and content of  $Mg^{2+}$  and  $Na^+$  ions. It is very important to note that these elements are generally implicated in the process of bone remodeling [32]. A detailed comparison between BioHA and synthetic HA materials can be found in Ref. [33].

In contrast to their excellent bone regeneration properties, CaP-based materials are brittle in bulk [34] (the brittle nature being in relation with their primary ionic bonds [3]), and characterized by poor mechanical properties. Their low impact resistance and tensile strength [35] represent critical drawbacks, which limit their wider clinical applications. However, the compressive strength value is rather good, exceeding that of the bone [35]. In general, an implant is fabricated from Ti or its medical-grade alloys. Despite their improved mechanical characteristics, Ti implants are characterized by low osseointegration rates. To overcome these shortcomings, HA can be used as a coating for Ti implants. This way, a combination between the ceramic's bioactivity and the metallic substrate's mechanical performances is attained [34,36]. To even accelerate coatings' osteoinduction and biomechanical fixation to the metallic substrate, some additions or HA doping with different ion concentrations were also reported [7,8]. Besides orthopedic prostheses and dental implants, HA coatings are currently being deposited also on (macro) porous scaf-

folds, thus expanding their applications towards bone regeneration therapies. Next to CaP, another important class of bioactive materials is represented by bioglasses (BG) [37,38], that demonstrated excellent osteointegrative characteristics in bulk form. Metallic implants' functionalization with BG coatings can be considered a good alternative for rapid bone repair and regeneration [39].

In the field of thin film growth, the PLD method proved to be a simple, versatile, fast-processing, and cost-effective technique, which allows for a precise control over the growth rate and morphology to fabricate high-quality coatings [40,41]. In the case of CaP-based biomaterials, one of the most important and enabling characteristics of this technique is its capability to grow stoichiometric films [41]. This is mainly due to a high ablation rate that causes the evaporation of all elements at the same time [42]. The deposition temperature, substrate position, or background pressure can be independently controlled for the ease of tailoring of the crystallinity, chemical composition, thickness and/or surface roughness of the fabricated structures [40]. One should emphasize upon that both film thickness and composition nonuniformity over high surface areas are two important drawbacks of the PLD technique, which can be fortunately overcome using special experimental set-ups (i.e., laser beam rastering over large diameter targets) [43]. In this respect, excimer lasers represent one economical choice for large-area commercial scale-up of the PLD process, advancing this technique as a viable alternative for future industrial applications [41].

There are studies in the dedicated literature on the *in vivo* testing of CaP-based coatings (especially HA) synthesized by many physical vapor deposition methods as alternatives to plasma spraying (PS), but only a few of them addressed the PLD technique. Moreover, to the best of my knowledge, there are no any review papers to summarize all the efforts dedicated in this direction, and the main objective of this review is to fill in this gap of knowledge. Therefore, the current review is focused on the gathering, compilation, and thorough discussion of the *in vivo* results pertaining to the studies reported in the last two decades on either synthetic or biological-derived CaP coatings only, synthesized by PLD technique, for various medical applications.

## 2. Search Strategy

### 2.1. Study Selection

A comprehensive literature search in the Web of Science (<https://apps.webofknowledge.com/>) database up to 11 December 2020, was carried out. The search included both animal- and human-related studies, and only the publications written in English were considered. The applied search strategy was: (“*in vivo*” [Topic], “Ti implants” [Topic], AND “Pulsed laser deposition” [Topic]), OR (“hydroxyapatite coatings” [Topic], “*in vivo*” [Topic] AND “Pulsed laser deposition” [Topic]), OR (“hydroxyapatite” [Topic], “Pulsed laser deposition” [Topic], AND “patient” [Topic]), OR (“hydroxyapatite” [Topic], “*in vivo*” [Topic] AND “Laser” [Topic]), OR (“hydroxylapatite” [Topic], “osseointegration” [Topic], AND “KrF laser” [Topic]), OR (“hydroxyapatite” [Topic], “osteoconduction” [Topic], AND “laser” [Topic]), OR (“calcium phosphate” [Topic], “*in vivo*” [Topic], AND “Pulsed laser deposition” [Topic]), OR (“calcium phosphate” [Topic], “*in vivo*” [Topic], AND “osseointegration” [Topic]).

### 2.2. Inclusion of Studies

These searches resulted in the identification of more than 700 studies. These titles were initially screened for possible inclusion, resulting in further consideration of approximately 100 publications. A careful screening of the abstracts led to 40 full-text articles. Considering the aim of this review, less than half of these articles (i.e., 15) met the inclusion criteria and were chosen and assessed in detail, and parts of the reported results were included and discussed in the present review.

### 3. Pulsed Laser Deposition Technique

Bioceramic coatings are currently used for various biomedical applications [9] to modify the implant surface (by increasing its surface roughness), to promote osseointegration. Nowadays, PS is the only industrial technology used for coating dental and orthopedic implants with CaP materials. In this respect, in the dedicated literature there are numerous and very interesting research works that point out and critically evaluate the physical-chemical and biological characteristics of the structures fabricated by this technique, along with their clinical performances [44,45]. The CaP-based coatings fabricated by conventional thermal PS onto medical implants function as an intermediate layer between the tissues and the metallic implants [46]. Despite its wide commercial availability, this technique still has some drawbacks, such as: (i) the synthesized coatings generally consist of several phases (i.e.,  $\beta$ -TCP forms at 1200 °C, and it transforms into TTCP at  $T > 1400$  °C); (ii) at higher synthesis temperatures, the negative influence of the mismatch between the thermal expansion coefficients of HA and TCP and the ones corresponding to Ti-based alloys ( $11\text{--}15 \times 10^{-6}$  cm/(cm·K) vs.  $8\text{--}10 \times 10^{-6}$  cm/(cm·K), respectively), limit the obtaining of good CaP coatings onto metallic substrates [47]; (iii) it supplies very thick structures with low adherence to the substrate (because the coatings' tensile stresses have a greater tendency to initiate cracks and cause film delamination [47]); (iv) surface morphology, phase composition, or uniformity of crystallization [32,48] are difficult to be controlled; and (v) it is a line-of-sight method [3]. Therefore, no coating technique can be considered perfect and all these drawbacks gradually supported research efforts focused on the introduction of various, alternative coating techniques to PS (i.e., radio frequency magnetron sputtering, PLD, electrochemical deposition, etc.) [1,3,7,8,11]. Among these, PLD technique is worth mentioning due to some important advantages over PS method, such as: (i) a much faster surface deposition process; (ii) a stoichiometric transfer of the material's composition from the target in the synthesized coating; (iii) a better morphological and compositional uniformity; (iv) a lower porosity; (v) precise thickness control; (vi) effectiveness for coating small implants, with complex shapes; (vii) a decreased tendency of the synthesized structures to crack or delaminate; and, very important, (viii) a high adherence to the metallic substrate [1,49]. In the biomedical field, for the fabrication of CaP-based coatings for bone implant applications, one of the most applied plasma-assisted methods is PLD [7]. This technique is able to fabricate dense and extremely adherent films. In this respect, synthetic HA and BioHA coatings obtained by PLD previously demonstrated high adherence to metallic substrates [50]. Moreover, the composition of these coatings is consistent with the one corresponding to the raw (base) materials, along with an improved crystallinity [50]. One should note that in PLD, after the ablation of the target by laser pulses, a plasma plume is generated. When the species existing in the plume reach the surface of the substrate, they may deposit onto the surface and form a film [41]. The number of the deposited species depends both on their density in the plume and their energy. In the case of low energies, the species may not deposit on the substrate surface even if they arrive at the surface [51]. If the substrate temperature is high, the energy of the species can be compensated. Consequently, the number of deposited species onto the substrate surface will increase, along with the density of the droplets. High substrate temperatures also contribute to the atomic diffusion, which, in turn, can determine the appearance of two phenomena: the first one is the atomic rearrangements and crystallization of the film and the second one, the improvement of the film–substrate bonding state [52].

The laser sources appropriate for the ablation of a wide range of materials use wavelengths in the UV domain due to some important advantages over IR and/or visible laser sources, such as (i) a higher penetration depth of the laser beam in the target material and (ii) a higher energy of the photons that allows for a more efficient vaporization of the target [53]. In this respect, the laser sources used for PLD experiments are either excimer lasers (i.e., ArF [54], KrF [55], or XeCl [56], emitting at wavelengths of 193, 248, or 308 nm, respectively) or solid-state lasers (i.e., Nd:YAG [57], emitting at 266 nm). It should be also emphasized that to increase the amount of evaporated material from the ablated target to

the detriment of expelled liquid or solid phases, lasers emitting in a pulsed regime with pulse durations in either the nanoseconds or picoseconds range are generally used [58]. In these regimes, the absorption process takes place more quickly than in the case of thermal diffusion processes. More insights on the PLD and PS techniques are well described elsewhere [33,41,49].

It is important to mention that post-deposition treatments are generally applied to transform CaP phases with lower Ca/P ratio to crystalline HA. Thus, there are two commercially used post-treatments: sintering [33,59,60] and soaking in alkaline solutions [61,62]. These treatments are generally applied for several hours, in the range of 600–800 °C. Their aim is to transform the water trapped in the film during the synthesis process in OH<sup>-</sup> ions, to stabilize the crystalline structure [34].

There are reports in the dedicated literature on the *in vivo* testing of CaP-based coatings (especially HA) fabricated by different physical vapor deposition methods, but, to the best of my knowledge, only a few of them addressed the PLD technique. Therefore, for an easy access to information, Table 1 introduces the PLD experimental details given in the papers considered in this review.

**Table 1.** Pulsed laser deposition (PLD) experimental details given in the papers considered in this review, in the chronological order in which they were reported in the literature.

Laser	Repetition Rate (Hz)	Substrate Temperature (°C)	Fluence (J/cm <sup>2</sup> )	Atmosphere/Pressure (Pa)	Coating Thickness (µm)	Post-Treatment	Ref
KrF	-	500	3	Ar–water vapor	1	-	[63]
KrF, CO <sub>2</sub>	2–10	RT	3–10	-	1–4	550 °C, 1 h, 10 <sup>-2</sup> Pa	[64]
KrF	-	490	3	Ar–water mixture	1–1.2	-	[65]
KrF	30	650–730	4–7	Ar/H <sub>2</sub> O/40–80	1–3	-	[66]
ArF	20	490	0.9	Water vapor/45	2	-	[67]
KrF	2	150–400	2	O <sub>2</sub> /13–50	0.4	150–400 °C, 6 h	[68]
ArF	-	460	4.2	Water vapor/45	0.05–0.1	-	[69]
-	-	-	-	-	0.05/0.3	800 °C, 8 h	[32]
ArF	10	RT	1	Water vapors/0.1	-	380 °C, 1 h	[70]
KrF	5	200,600	5	Ar/45	-	-	[52]
KrF	10	400	5	Water vapors/50	-	400 °C, 6 h	[71]
-	3	186,410	4.6	Water vapors	-	-	[72]
KrF	-	-	-	-	-	-	[73]
KrF	5	600	5	Ar/45	-	-	[74]
KrF	10	500	3.5	Water vapor/50	-	600 °C, 6 h	[75]

#### 4. In Vivo Assessment of PLD CaP-Based Coatings

*In vitro* tests play key-roles in the overall evaluation of a biomaterial by delivering important information on its potential behavior inside a living system. To better understand the complex processes occurring in a living environment and to deliver accurate data for the validation of the biomaterials' performances that target clinical trials, *in vivo* tests (using either animal or human models) are of key-importance and should, therefore, follow thorough *in vitro* acceptance [75].

Biocompatibility is an essential and required characteristic of the biomedical materials introduced inside the living systems, presenting a beneficial interaction with the surrounding bone tissues. Immediately after CaP-based functionalized implants are surgically inserted into the living bodies, there are tissue responses that take place at the implanted materials–soft/hard tissues interface. The formation of connective tissue fibers (2–3 weeks), which make a fiber mesh containing carbonated apatite, is one such response that occurs initially [76,77]. This tissue-free layer develops onto the ceramic surface and actively contributes both to a strong fixation of the implant to the surrounding bone tissues and to the acceleration of bone integration and healing at early implantation times [78–81]. These aspects are of key-importance for any implant system [82]. The amount and nature of osseointegration in metallic implants are determined by several factors such as surface

topography, which includes surface roughness [83], wettability [84,85], and surface morphology [86,87]. It was demonstrated that an initial stability and a further stronger interface with the bone tissues are more likely to be achieved in the case of implants with rough surfaces as compared to smooth ones [88], in both animal and human models, with bone ongrowth interface [89,90]. Furthermore, the bone–implant interfacial shear strength is directly related to the degree of surface roughness. However, for an optimal clinical performance of metallic implants in bone, both an ideal type/shape of the implant and the surface roughness degree still remain unknown. It is also important to mention that initial stability is also achieved by drilling the bone socket to a diameter slightly inferior to the implant's dimensions, but to the proper matching length of the implants. If the opening hole is drilled through the bone and enlarged progressively, and the implant is screwed in with low momentum, the surrounding bone is going to be compressed. This provides a firmer fit to the implant itself and it also increases the calcium concentration in the interface. This method decreases also the blood clot thickness around the implants. If growth factors are used, a boost in the healing process will be observed, while in their absence, the osteoconduction process only will occur.

A nowadays challenge in implantology is the capability of a surface to assist cells' colonization and differentiation. Cell migration, adhesion, and proliferation onto implant surfaces are key-processes for the initiation of tissue regeneration [91]. Osteoconduction and osseointegration represent two mechanisms that involve the adhesion or proliferation of cells and integration in the CaP [35,92]. The adhesion of cells is directly related to the CaP ability to adsorb the proteins from the extracellular matrix. For CaPs, this is strongly determined by important parameters, such as the surface roughness, crystallinity degree, Ca/P ratio, solubility, phase content, grain and particle sizes, and surface energy [92].

Osteoinduction is the property of a material to induce the differentiation of progenitor cells to osteoblasts [35,92]. It was demonstrated that CaPs in the absence of supplements are osteoinductive materials [92]. In turn, the osteoinduction ability depends on several CaP properties, i.e., surface charge, morphology, and chemistry, which can influence the adsorption of proteins [92].

The success rate of a medical implant is in relation to several factors such as the implant's design, the structure, and properties of the used material, the applied loads' magnitude, the employed surgical technique, health conditions of either animals, or human patients [82], and the existence of an inflammation-free environment. In the latter case, there exist two major problems: (i) the area intended for the implant insertion might be infected and (ii) the implant's surface might get contaminated during surgery. Both situations can be easily by-passed, by appropriate dental work and by a proper isolation during the surgical act, respectively. All aspects related to the biological interactions to improve the long-time stability and reliability of medical devices inside living systems have pushed forward the research of a wide range of surface modification techniques. The aim was to achieve rapid healing and an improved bone-implant interaction, for an early osseointegration. Therefore, in the last two decades, the surface functionalization of implants by increasing the bioactivity using various biological and chemical processes or by surface macro- and microtexturing was one of the major research topics in the biomedical domain [82].

#### 4.1. Used Substrates

Currently, in comparison to polymers and ceramics, metallic biomaterials are extensively used in orthopaedics, dentistry, and oral and maxillofacial surgeries. This is due to several important advantages, such as the high mechanical strength, superior biocompatibility, high resistance to corrosion, and improved chemical stability under biological conditions [93–95]. Bioinert metallic implants (i.e., stainless steel (316L) and Ti, Ti-based, and cobalt-chromium alloys [96]) are generally utilized for a wide range of medical applications, but there is currently a new generation of biodegradable metals (i.e., Mg, Zn or Fe) that has been intensively employed for temporary applications [97,98]. Because they do

not chemically bond to bone tissue unless their surfaces are modified, the use of the latter ones is generally limited.

#### 4.2. Animal and Human Implant Models

After the *in vitro* validation of biomaterials' surfaces, the use of laboratory *in vivo* models is a step forward biocompatibility assessment [99] and future clinical outcome of metallic implants introduced in bones. In this respect, *in vivo* testing on animal models is a key-parameter for both understanding and evaluation of the biological processes that occur in a living system.

The general animal spectrum used for *in vivo* testing of CaP-based coatings synthesized by the PLD technique only is limited to rats, rabbits, (mini) pigs, dogs, goats, and sheep [34], and each animal model having its own advantages and limitations [100]. Small animal models demonstrated some important advantages over larger ones, i.e., overall lower costs, osteogenic ability, the possibility to both shorten the implantation time-periods [101,102], and monitor bone formation by imaging methods (e.g.,  $\mu$ CT). Thus, the possibility to carry out longer experimental times is worth considering. In this respect, rat or mice models are generally used for subcutaneous examination of implants [103,104], while rabbits represent the easiest way to investigate the interaction between the coating and the femoral bones [105–107]. It should be noted that the rabbit bone model was previously indicated [108,109] as a valuable screening tool able to select favorable implant surface characteristics/technologies before moving to the next step (i.e., human trials). It is currently used in various medical tests [110], due to both its size and ease of handling. In addition, it was demonstrated that its skeleton reaches maturity very fast (~24 weeks) [111]. In comparison, large animal models (i.e., dogs, sheep, or goats) are generally indicated for verifying the practicability of implants closer to real clinical situations. In such large animal models, the investigation of the osteoinduction process is easier to be attained than in the case of small ones. Large animals have the advantage of an immune system more similar to humans than in the case of small animals and can offer the possibility to host different types of test materials [112]. Despite this, such large animal models are not so intensively utilized for the evaluation of osteoinduction because of their lower metabolic rates, besides higher costs for management and maintenance [113].

Usually, implants are surgically inserted in either the femur, tibia, or mandible bones [114]. The rabbit's bones manifest faster changes as compared to the case of larger animal models [115]. Considering the difficulties met when extrapolating the results obtained on rabbit bones to the human case, various screenings for implant design and validation of the tested materials are still needed to be performed [75], before their testing on larger animal models. Dog models are generally used for testing dental implants [116]. One should emphasize upon that the focus of the most studies is directed to the biological response of the living bone to CaP-based materials.

For an easier follow-up of the text, Table 2 introduces information on the sample codes, which will be further used in the paper.

For an ease access to information presented in the papers considered in this review, Tables 3–6 introduce data on the investigated coating materials (along with the type and dimension of substrates, bone implantation sites, length of studies, and all performed analyses). All the information was grouped according to the applied small and large animal models, respectively (Table 3—rats/mice, Table 4—rabbits, Table 5—minipigs, and Table 6—dogs/sheep/humans).

It should be emphasized that because of the reduced number of *in vivo* studies on the PLD synthesis of CaP-based coatings, the use of a certain animal model as the most suitable one for the optimal assessment of metallic implants' osteoconduction has not been established yet. The reports on clinical trials (using human patients) are therefore scarce [71].

**Table 2.** Sample acronyms related to different materials used in the review and their explanation.

Samples Code	Description of Samples
Ti/Ti6Al4V	Titanium/titanium alloy (control specimen or deposition substrate)
HA	Synthetic hydroxyapatite
HA/TTCP	Synthetic hydroxyapatite/tetracalcium phosphate
OCP	Octacalcium phosphate
Mn-CHA	Manganese-doped carbonated hydroxyapatite
BHA/HA	Bilayer bovine hydroxyapatite/hydroxyapatite
HATW	Titanium web scaffold functionalized with hydroxyapatite
HA/45S5; HA/BG	Hydroxyapatite/bioglass composite
Mg:OCP	Octacalcium phosphate doped with magnesium
Mg:HA	Synthetic hydroxyapatite doped with magnesium
FHA	Fluoridated hydroxyapatite
Li-C	Biological hydroxyapatite doped with lithium carbonate
Li-P	Biological hydroxyapatite doped with lithium phosphate

**Table 3.** Information related to the investigated coating materials, according to the applied small animal models (i.e., rats/mice).

Investigated Material	Animal Model/Number	Used Substrate/Dimensions	Bone Implantation Site/Length of Study (Weeks)	Performed Analyses	Ref
HA	Adult rats/36	Teflon, polyethylene, Ti6Al4V/2.5 × 2 × 1 mm <sup>3</sup>	Femurs/2–8	SEM, histology	[64]
HA	KSN nude mice/12	Ti web discs/5 mm diameter, 1.5 mm thickness	Backs/2–12	Histology	[70]
Fluoridated HA	Rats/16	Ti disc implants and screws/15 mm diameter, 1 mm thickness and 1.2 mm external diameter, 12 mm length	Distal femur/4–8	Microcomputed tomography, histology	[73]

**Table 4.** Information related to the investigated coating materials, according to the applied small animal models (i.e., rabbits).

Investigated Material	Animal Model/Number	Used Substrate/Dimensions	Bone Implantation Site/Length of Study (Weeks)	Performed Analyses	Ref
HA, HA/TTCP	New Zealand White Rabbits	Ti6Al4V	Proximal tibia, distal femurs/8	Histomorphometry	[66]
HA	New Zealand White Rabbits/12	Grit-blasted commercial titanium rods/7 mm length, 2 mm diameter	Proximal tibia/24	Histology, histomorphometry	[67]
HA, Mn-CHA, OCP	New Zealand White rabbits/12	Coins of Ti implants/1.95 mm thick, 6.25 mm diameter	Tibia/8	Tensile (pullout) tests	[68]
HA/45S5	New Zealand White rabbits	Ti6Al4V/20 mm diameter, 1 mm thickness	Shin bones/4–12	Histology	[52]
Mg-doped octacalcium phosphate and HA	Rabbits/23	Porous Ti6Al4V scaffolds/(10.3 × 2.5 × 2.5) mm <sup>3</sup>	Femoral condyles/24	Histopathology, planimetric analysis, $\mu$ CT	[72]
HA/45S5	New Zealand White rabbits	Ti6Al4V plates/ $\Phi$ 20 mm × 1 mm	Shin bones/4–8	Histology	[74]
Lithium-doped biological HA	New Zealand White rabbits/26	3D Ti implants/3.5 mm internal and 5.5 mm external diameters, 9 mm length	Femoral condyles/4–9	Computed tomography, mechanical testing, scanning electron microscopy	[75]

**Table 5.** Information related to the investigated coating materials, according to the applied small animal models (i.e., mini-pigs).

Investigated Material	Animal Model/Number	Used Substrate/Dimensions	Bone Implantation Site/Length of Study (Weeks)	Performed Analyses	Ref
HA	Mini-pigs/3	Dental cylindrical implants/13 mm length, 3.3 mm diameter	Lower jaws/16	(Micro)radiography, transmission and fluorescent microscopies	[63]
HA	Mini-pigs/4	Ti6Al4V dental implants/12 mm length, 3.3 mm diameter	Lower jaws/16	Polarized and fluorescent light, percentage of osseointegration	[65]

**Table 6.** Information related to the investigated coating materials, according to the applied large animal models (i.e., dogs/sheep/human patients).

Investigated Material	Animal Model/Number	Used Substrate/Dimensions	Bone Implantation Site/Length of Study (Weeks)	Performed Analyses	Ref
BHA/HA	Beagle dogs/8	Commercial Ti screw implants/8 mm length, 3.7 mm diameter	Bilateral femoral Shafts/4–24	Histology	[32]
HA	Sheep/20	Cylindrical Ti implants/10 mm long, 5 mm diameter	Tibia/8–12	Histomorphometry	[69]
HA	Human patients/12	3D Ti mesh implants/(10 × 5) cm <sup>2</sup> size, 0.2 cm in holes diameter, thickness of 0.25 cm	Skulls/12–24	Tomodensitometry	[71]

#### 4.3. Characterization Methods

For the *in vivo* assessment of the CaP-based coatings considered in this review, the performed investigations, on which we will focus our attention, are standardized radiography, microradiography, (micro) computed tomography ( $\mu$ CT), tomodesitometry, histology (under polarized and fluorescent light), histomorphometry, planimetric analysis, fluorescent microscopy, scanning and transmission electron microscopies (SEM, TEM), and mechanical testing. While mechanical testing aims to determine the bonding strength between the newly formed bone tissue and the implant, histological investigations are used for a wide range of purposes, such as the measurement of the new bone area, bone apposition ratio, etc. [105–107,117]. It is important to note that light microscopy or optical microscopy is the most common laboratory technique used for biological investigations. It is a cheap, robust, and typically noninvasive method that uses visible light to detect and magnify small objects. The resolution limit is an intrinsic property due to the wavelength of visible light radiation [118]. Polarized light microscopy is a contrast-enhancing technique with a high degree of sensitivity that can be used for both qualitative and quantitative investigations. It can provide information on both absorption color and optical path boundaries and the structure and composition of materials that are invaluable for identification and diagnostic purposes. The technique of fluorescence microscopy has become an essential tool in biology and biomedical sciences, as well as in materials science, being capable of revealing the existence of single molecules. SEM and TEM microscopies enable the characterization of microstructures at many different length scales, from micro- to nanoscale, within an imaging session. They all generate a highly focused beam of electrons, which impacts the specimens inside a vacuum chamber. SEM microscopy is used to examine material surfaces, in comparison to TEM microscopy, which primarily focuses on investigation of the internal structure of the specimens [118].

##### 4.3.1. Standardized Radiography and Microradiography

Dostalova et al. [63] evaluated quantitatively and qualitatively the Ti implants by radiographical measurements. After 16 weeks of implantation, the osseointegration process was confirmed by the presence of newly formed bone around all implants, along with a strong bone–implant connection. When measured in the long-axis cross-section, the implant area

was in the range of ~25–28 mm for Ti implants and ~21–37 mm in the case of the HA-coated ones. This corresponded to an osseointegration area of ~18–22 mm for Ti implants and of ~15–30 mm for the HA-functionalized ones. The inferred percentage of osseointegration varied from 73% to 79% for Ti implants and from 70% to 86% for the HA-coated ones. No differences between various implants were found to be statistically important.

#### 4.3.2. Computed Tomography

Using  $\mu$ CT, Mroz et al. [72] performed qualitative and quantitative investigations on Mg:HA samples and Ti implants, and the obtained results revealed significantly higher differences between these groups ( $p = 0.0311$ ).

In another study, Chen et al. [73] demonstrated by  $\mu$ CT that for both 4 and 8 weeks, the ratio of bone volume to total volume, mean trabecular number, and mean trabecular thickness were significantly higher ( $p < 0.05$ ) in the case of FHA-coated implants, which was indicative for an accelerated osteogenesis process in the region of interest. Moreover, for both time periods, the mean trabecular separation was found to be significantly lower ( $p < 0.05$ ).

Duta et al. [75] used CT scans, at 4 weeks after the surgical procedure, to observe the correct placement and the good integration of all implants into the surrounding bone. Thus, the presence of the peripheral osteosclerosis and no inflammatory process of the soft tissues were indicated. The obtained results pointed out to an increase in the osseous density, for both investigated time periods (4 and 9 weeks, respectively). Thus, the bone density values corresponding to the Li-C and Li-P coatings, measured at 9 weeks, were ~1.2 times higher than those inferred at 4 weeks after implantation. At 4 weeks, both Li-C and Li-P structures indicated bone density values ~1.3 times higher than those obtained for Ti implants. Moreover, at 9 weeks, the density values inferred in the case of functionalized 3D Ti implants were ~1.4 times higher as compared to Ti ones.

#### 4.3.3. Tomodensitometry

In a pioneering contribution, Duta et al. [71] used the tomodensitometry analysis to evidence the osteogenesis process of simple and functionalized Ti meshes implanted in human patients, at 3 and 6 months after surgery. After 3 months, no changes were detected for any of the investigated patients in terms of tissue density on Hounsfield (HU) scale. After 6 months, in the case of two patients with Ti mesh and for all with Ti meshes functionalized with bioactive surfaces, changes in measurements of osteoinductive and osseointegration phenomena were evidenced. In the first case, these changes were assessed only on the edge area, which was in direct contact with the bone. In the second case, four patients from the total of six, showed changes of tissue density, both on the edge and interjacent areas of the mesh. Up to 6 months, no patient evidenced those changes in the center region of the implants. Thus, the inferred values for the functionalized Ti meshes were of 583 and 412 HU (for the edge and interjacent region, respectively), in comparison to 78 HU, obtained in the case of Ti meshes.

#### 4.3.4. Histology

Antonov et al. [64] performed histological evaluations of their synthesized structures for three different time periods of 15, 30, and 60 days, respectively. It is important to note that no inflammation was observed around the sites of implantation for any of the investigated structures. However, in the case of Ti samples, a significant fibrous tissue formation was pointed out. For both types of structures (synthesized by either KrF or CO<sub>2</sub> lasers), a thin fibrous layer could be observed after 15 days of implantation. At 30 days, a partially direct bone–implant contact was indicated, while very little fibrous tissue and the formation of new bone, which was in direct contact with the implant surface, were shown at 60 days. A very interesting observation was that the osteointegration rate was slightly superior in the case of annealed samples, rather than for the non-annealed

ones. Between the two types of synthesized coatings (using either KrF or CO<sub>2</sub> lasers), no significant statistical differences in the osteogenesis process were inferred.

The histological evaluation under polarized and fluorescent light was used by Dostalova et al. [65] to indicate the presence of newly formed bone tissue around the investigated implants. No osteoclasts, macrophages, or any inflammatory reaction cells could be observed in the ground sections. In the case of synthesized coatings, a fibrous connective tissue occurred in ~23% of the implant surface, but without the formation of a continuous layer. In contrast, the fibrous connective tissue between the implant and the newly formed bone tissue occupied ~35% of the surface, especially in the middle part of the implant. However, it was indicated that these differences were not statistically significant ( $p = 0.05$ ). Under fluorescent light, a uniform distribution of the fluorescent label in the whole bone, most probably due to a remodeling process of early formed bone, was observed. These results were supported by the higher magnification investigations, in which active bone cells were observed.

Using histological analyses, Peraire et al. [67] succeeded to demonstrate bone up-growth in the endosteal areas, with a great amount of lacunae area in contact with them, while in the center, the bone apposition was indicated to be totally absent. The fiber mesh either disappeared in some implants or was very thin. In the case of the Ti rods functionalized with HA coatings by plasma spraying (HA-PS), a good bone regeneration at the ends of the implants (endosteal zones) was observed, but the newly formed bone tissue in contact with the implant surface evidenced a significant large amount of lacunae area. This active remodeling process might occur because of the coating degradation. HA-PS coatings partially disappeared in some areas of the implants, were delaminated or even detached, and HA particles could be therefore observed. In the central zone, bone apposition areas could be hardly seen, with a slightly thicker fiber mesh. Inflammatory cells (i.e., lymphocytes, macrophages, or neutrophils) were also present. In the case of HA coatings synthesized by PLD (HA-PLD), a good bone regeneration at both endosteal ends of the implant was indicated. All samples presented superior (grade 4) responses in bone reaction and interface analysis parameters. The newly formed bone tissue was similar to the cortical one, and the presence of mature osteocytes was detected. Under optical microscopy, HA-PLD coatings could not be evidenced because of their low thickness, while under polarized microscopy, the mineralized matrix in apposition to the implants could be observed for all investigated areas (cortical insertion area, opposite endosteal area, and bone marrow). The central area in contact with the bone marrow indicated bone apposition areas interspersed in a thin fiber mesh, with large trabeculae growing from the coating surface.

Hayami et al. [32] performed histological investigations of the interface between bone and the tip of each implant. After 4 weeks, large gaps at the Ti implant–bone interface could be observed, bone and connective tissues being intermingled. In the case of the sprayed implants, a thick adhering coating could be clearly seen, along the observable length of the interface. For the BHA/HA bilayered implants, no detectable gap was visible, and the bone and the implant closely adhering to each other along the full length of the interface. Thus, the process of biointegration was assumed to be complete after only 4 weeks of implantation. This strong bone–bilayered implants connection was also observed at 8 and 24 weeks post-operation. At 24 weeks after surgery, normal bony structures with osteocytes were indicated surrounding the implants.

Using histological analysis, Hontsu et al. [70] could observe that the HA-functionalized implants were surrounded by a mesh of thin fibrous tissue. Inside the implants, the mesh porosity was filled with fibrous tissue containing capillaries. Inside the HATW structure, a slight amount of new immature bone formation was indicated. This amount clearly increased from the second to the fourth week of implantation, for all types of scaffolds. At 4 and 8 weeks, more sites containing osteoblast-like cells and osteoid tissue expressing active bone formation could be observed, while at 12 weeks, the structure of the bone was further matured and contained larger areas of remodeled lamellar bone.

After observing the stained tissue sections, Wang et al. [52] indicated an obvious crack between the newly formed bone tissue and the 200 °C-synthesized film. This was mainly because of the preparation process of the tissue sections.

Although SEM results demonstrated good connections between the newly formed bone tissues and the surfaces of the two type of films (Figure 1a,b), the histological micrographs indicated a superior bone growth of the structures synthesized at 600 °C, in comparison to those prepared at 200 °C. The osteoblasts in the newly formed bone tissue were shown clear and homogenous, with a growth oriented along certain directions.

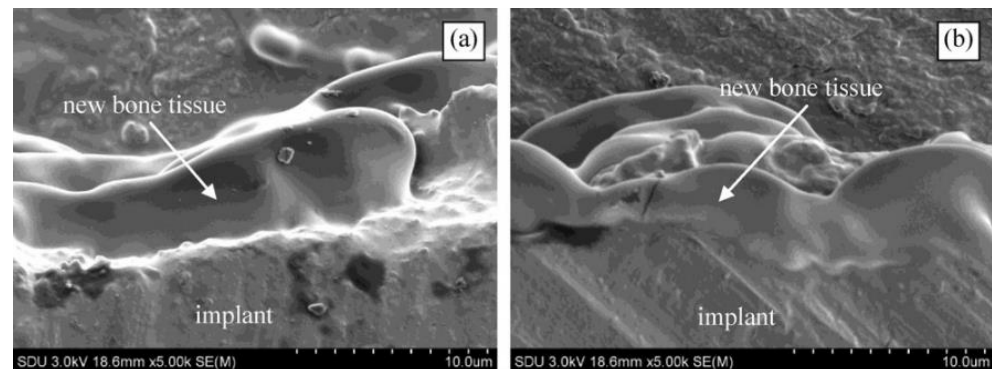


**Figure 1.** Morphologies of the implants after embedding for 1 month. (a,b) are the SEM morphologies of 200 and 600 °C films. (Reprinted with permission from [52]. Copyright 2013 Elsevier.)

It was therefore concluded that all tissue sections from the implants deposited at 600 °C were good, with a satisfactory connection between the film and newly formed bone tissue. In contrast, for the structures synthesized at 200 °C, a lower adherence between the newly formed bone tissue and the films was demonstrated. This was mainly influenced by the presence of a dark area between the film and the new bone tissue, which seemed to appear because of the high shearing stress during the cutting process.

Using the histopathological evaluation, Mroz et al. [72] showed that Ti implants had a tight adherence to the mineralized bone tissue, being in many cases within the fatty marrow. Small fields of connective tissue were also observed directly adjacent to the implant, along with a direct penetration of regular bone into the implants' pores. In the case of Mg:OCP samples, a direct integration of the bone and penetration into the pores and the structure of the implant were indicated. For the Mg:HA group, evidence of a direct bone–implant integration was shown, with no sign of osteoclastic or osteoblastic reaction around the implants.

Longitudinal sections were collected by Chen et al. [73] to assess the newly bone tissue formation around the implants. No adverse inflammatory reactions or gaps at the bone–implant interface were observed. At 8 weeks after surgery, the bone area ratio and bone–implant contact were significantly higher (~6 and ~1.5 times, respectively) around FHA-coated implants in comparison to Ti ones.

Wang et al. [74] performed histological investigations to assess the osteoconduction capacity of HA/BG composite coatings, with three different BG concentrations. Thus, the 90%HA + 10%BG structure was shown to connect well with the bone tissue. However, the bone matrix filled the implant–bone tissue interspace, and osteoblast cells (OB) were not observed in this region before 2 months after implantation. In contrast, the 80%HA + 20%BG film exhibited better osteoconduction behavior as new OB could be observed near the implant surface in the first month after surgery. It is important to note that the improved biological activity of the film was indicated to be mainly due to their *c*-axis orientation. Macroscopically, a good connection with the bone tissue was also observed in the case of the 20%HA + 80%BG structure. In this case, a crack was indicated between the film and the bone tissue, which corresponded to a poor bond state (mainly because of the shearing force coming from the inner circle saw, used to cut the specimen into slices).

#### 4.3.5. Histomorphometry

Dostalova et al. [65] inferred the area of the bone–implant interface and found the values to vary from ~65%, for Ti implants, to ~78%, for HA-functionalized ones. It is important to note that between both types of surfaces, no significant statistical differences were inferred (Student's *t*-test,  $p = 0.05$ ). As a consequence, a similar osseointegration trend for both Ti implants and HA-functionalized ones was indicated.

In the case of the implants inserted by Kim et al. [66] in the femur, a value of ~48% of the mineralized bone at the bone–coating interface for the synthesized HA coatings and of ~63% for the HA/TTCP biphasic ones, was inferred. For the case of tibia-implanted samples, values of ~51% and ~56% for the mineralized bone were indicated in the case of HA and HA/TTCP biphasic coatings, respectively. Very important, all samples were shown to exhibit a good integration, with no significant foreign body response.

Among the three materials evaluated by Peraire et al. [67], there were no statistically significant differences in bone in-growth around the drilling hole. However, the HA–PLD implants presented the highest value of the percentage of bone contact (86%), and the lowest value of percentage of lacunae contact (14%). This difference was statistically significant (Scheffe Test,  $p < 0.05$ ). When referring to the ratio between the total bone surface and length of the evaluated area, the HA–PLD implants showed a significant increase in comparison to the HA–PS group (Scheffe test,  $p < 0.05$ ). This did not apply as well to the Ti group. In the case of the HA–PS group, even though the bone response was slightly different than the one corresponding to the Ti, no statistically significant differences were found, in any of the quantified variables.

Paz et al. [69] used in their study two methods to evaluate the percentage of bone–implant contact (% BIC): conventional light transmission microscopy and environmental scanning electron microscopy (ESEM). The obtained results demonstrated no statistically significant differences between these two methods, although ESEM is believed to offer greater precision when characterizing bone areas in close contact with implant surfaces. ESEM analysis showed a considerable improvement of the bioactivity in the case of HA-coated samples, the bone–implant interface being more homogeneous and continuous in comparison to Ti implants. Moreover, the bone was observed to enter deeper into the craters of the macrostructure for the HA-coated samples than for the Ti implants. In areas with low bone density, the HA-coated structures presented a superior behavior in contrast to Ti. ESEM analyses showed an improvement of the percent of total BIC for both HA-synthesized coatings (50 and 100 nm-thick samples, respectively) with regard to Ti implants. There were no significant differences between the two coated samples, although the percent apical BIC indicated better characteristics of the thicker coating over the thinner one. The conventional light transmission microscopy images showed similar results as ESEM, but with a modification in the percent total BIC; for this investigation, the thinner HA coating showed superior behavior in comparison to the thicker one, while for the percent apical BIC, the thicker coating presented a better behavior, but with a great increase in the standard deviation for the thinner one.

#### 4.3.6. Planimetric Analysis

The results of planimetric investigations performed by Mroz et al. [72] revealed the best bone integration in the case of Mg:HA samples, this group having the highest average length of the bone–implant interface and also the best reproducibility of the results. No significant differences were inferred between the Mg-doped (OCP and HA) implants and the Ti ones.

#### 4.3.7. Fluorescent Microscopy

When fluorescent microscopy was used by Dostalova et al. [63], the active bone formation could be observed, both in the neck and in the bottom of the implants, surrounding osteons and braiding the fibrous connective tissue on the implant.

Chen et al. [73] investigated by fluorescence microscopy the bone formation around the implanted structures. As determined by confocal laser scanning microscopy, the bone area between the implant surface and the boundaries observed at 1, 4, and 8 weeks, respectively, was significantly higher for FHA-coated implants as compared to Ti ones ( $p < 0.05$ ). These implants indicated 1.5 and more than 4 times more new bone tissue formation at 1 week and 4 and 8 weeks, respectively, as compared with the case of Ti implants.

#### 4.3.8. Scanning Electron Microscopy

Antonov et al. [64] used SEM to investigate the in vivo behavior of the synthesized coatings. New bone formation was therefore observed, which surrounded implantation site of the HA-coated alloy samples.

SEM observations performed by Peraire et al. [67] allowed for the detection of the HA-PLD coatings on the grit-blasted Ti surfaces, at 24 weeks after surgery. The images obtained using backscattered electrons showed different contrasts for the bone and the coating, which allowed for their clear differentiation.

Hayami et al. [32] investigated by SEM the holes from the removed implants. Because the threads of the screw implants had a long pitch, the troughs left in the bone were trapezoidal in shape. For Ti implants, bone growth was slow and insufficient because of the imperfect trapezium formation, in comparison to the BHA/HA-bilayered implants, where the growth rate and quantity of newly formed bone tissue were greater due to the formation of regular trapezia. In the V-shaped groove of the thermal-sprayed HA coatings, a flaky piece was indicated, which appeared to be a fragment that peeled away from the substrate.

Wang et al. [52] investigated the morphologies of the implants at 1 month after implantation. These are shown in Figure 1a,b.

A layer of newly formed bone tissue was clearly seen, developing along both types of structures (synthesized at 200 and 600 °C, respectively). This layer intimately adhered to the implants' surface and had a thickness of ~5 µm. After 3 months of implantation, the newly formed bone tissue occupied the bone–implant interspace (Figure 2a,b).

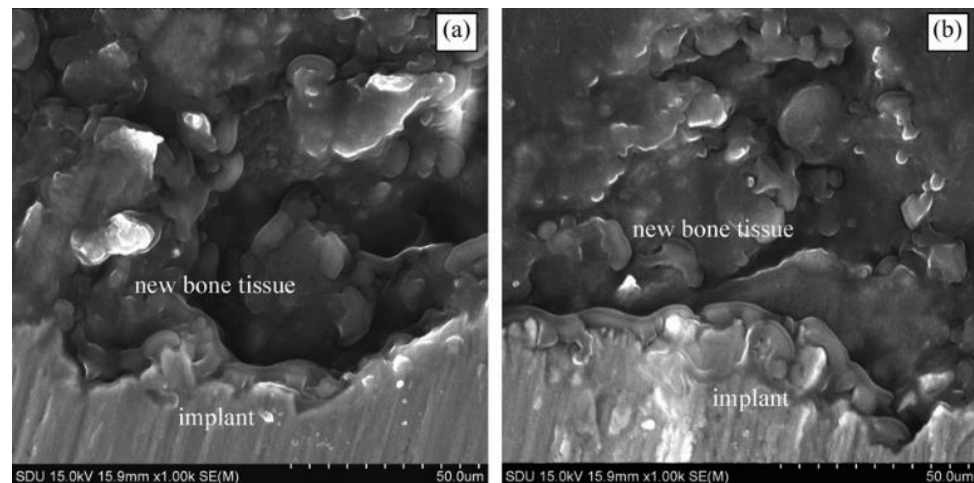


**Figure 2.** Morphologies of the implants after embedding for 3 months. (a,b) are the SEM morphologies of 200 and 600 °C films. (Reprinted with permission from [52]. Copyright 2013 Elsevier.)

A good bioactivity of the films was therefore indicated, the two types of implants being capable of inducing new bone growth on their surfaces.

Using SEM (Figure 3), coupled with the analysis of backscattering electrons, Duta et al. [75] managed to infer the adherence ratio of the remaining bone fragments onto the surface of the extracted implants.

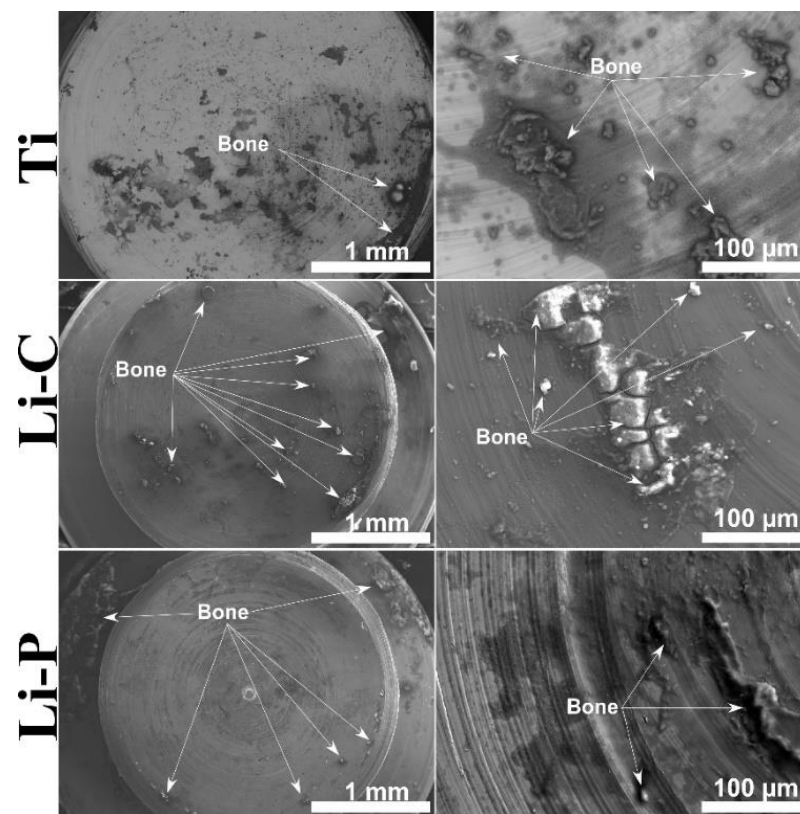


**Figure 3.** SEM micrographs indicating bone detachment on the surface of a control and functionalized (with Li-C and Li-P coatings) Ti implant, at 4 weeks after surgery.

Thus, adherence ratios up to ~38% higher in the case of functionalized 3D Ti implants (with Li-C and Li-P coatings) as compared to the Ti ones were indicated. This result, corroborated with the higher values of the detachment force obtained in the case of functionalized 3D Ti implants, in comparison to Ti ones, were indicative for an enhanced osseointegration process. Moreover, the presence of such osseous structures onto the surface of the implants suggested, besides the beginning of the implant integration process into the bone, the absence of any adverse reactions at the implantation site.

#### 4.3.9. Transmission Electron Microscopy

Using TEM, Dostalova et al. [63] have shown no marks of irritation and inflammation in the surrounded bone. OB could be seen both in the border of the implants and newly formed bone tissue. A low number of foreign body cells were indicated in the close vicinity of the implant cover. In the case of Ti implants, a fibrous connective tissue between the implants and the newly formed bone was seen, while in the case of the synthesized HA coatings, this layer could be observed only seldom.

#### 4.3.10. Mechanical Testing

The pullout (tensile) test was used by Mihailescu et al. [68] to compare the strength of the biological–chemical bonding between the bone and Ti implant surfaces functionalized with HA, Mn-CHA, and OCP coatings, respectively. The inferred values for all three tested groups demonstrated a significantly improved bone attachment strength value ( $p \leq 0.05$ ), which was about twice as high as the one associated to the Ti implants (~5 N). In comparison to the strength value corresponding to the synthetic HA (~8 N), up to 10% (in the case of OCP, ~9 N) and 25% (in the case of Mn-CHA, ~11 N) higher values were obtained.

Duta et al. [75] evaluated the quality of the implants' osseointegration by mechanical (tensile) tests. In none of the cases, alteration or disruption of the implants were present.

The detachment force ( $F_{\max}$ ) of implants under tensile pull-out testing, inferred for Ti and functionalized (with Li-C and Li-P coatings) 3D Ti implants, at 4 and 9 weeks after surgery, are represented in Figures 4 and 5, respectively.

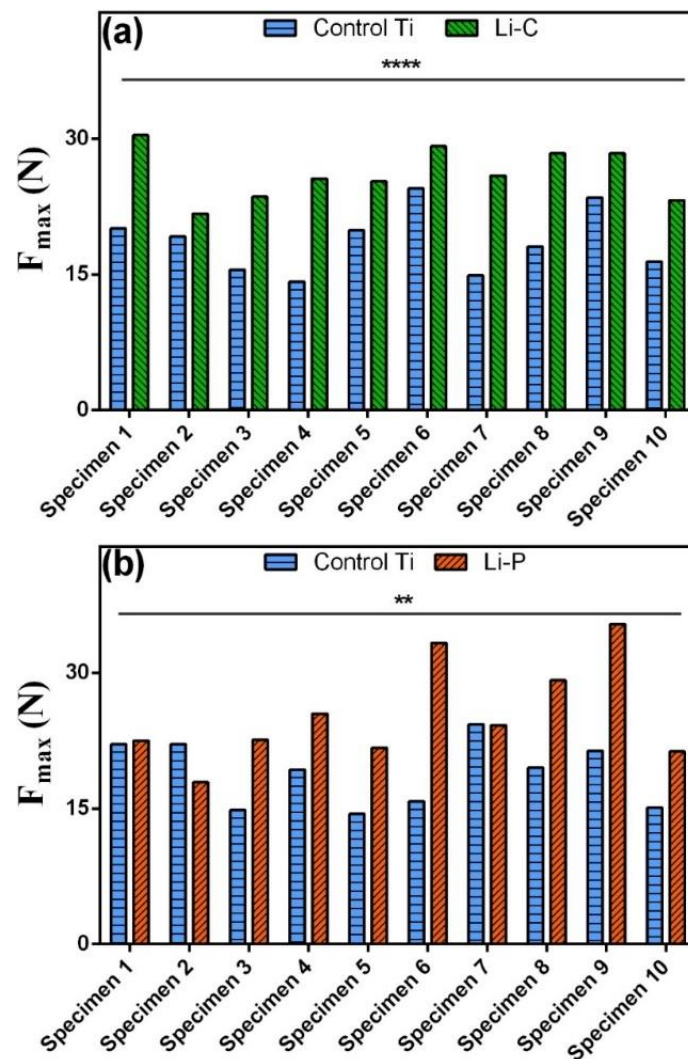


**Figure 4.** Detachment force,  $F_{\max}$ , of implants ( $n = 10$ ) under tensile pull-out testing, inferred in the case of control 3D Ti implants (marked in blue color) and of those functionalized with (a) Li-C (marked in green color) and (b) Li-P (marked in orange color) coatings, at 4 weeks after surgery. \*\*\*\* Represents highly significant differences ( $p \leq 0.0001$ ). \*\* Represents significant differences ( $p \leq 0.01$ ).

At 4 weeks after surgery (Figure 4), the obtained mean detachment force values demonstrated significant and highly significant differences between the Ti group and the Li-P one, and between the Ti group and the Li-C one, respectively. When referring to the extractions performed at longer periods of time, i.e., 9 weeks from implantation (Figure 5), the inferred mean detachment force values indicated highly significant differences for both investigated groups.

It is important to mention that the failure loads of the implants functionalized with both Li-C and Li-P coatings measured at 9 weeks were  $\sim 5$  times higher in comparison to those inferred at 4 weeks after surgery, respectively. Moreover, for both time periods, the Li-C and Li-P functionalized implants demonstrated a bone attachment strength of  $\sim 2$  times stronger than the one corresponding to Ti implants. One could therefore indicate that both the PLD surface functionalization of the implants and a longer implantation time

period could induce a positive influence on the overall bone bonding strength characteristics of the investigated medical devices. It should be emphasized that the fabrication of novel BioHA implant coatings derived from sustainable and inexpensive CaP resources, with improved mechanical properties, correlated with an increased bone fixation in vivo, could stand for a pioneering contribution to the progress of advanced medical devices.

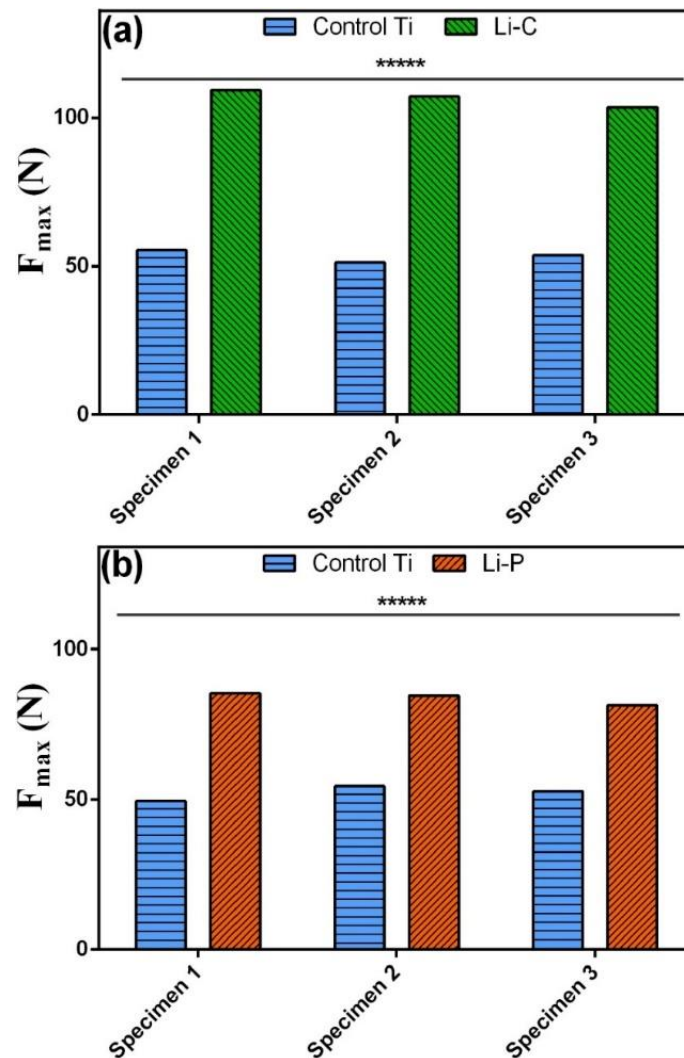


**Figure 5.** Detachment force,  $F_{max}$ , of implants ( $n = 3$ ) under tensile pull-out testing, inferred in the case of control 3D Ti implants (marked in blue color) and of those functionalized with (a) Li-C (marked in green color) and (b) Li-P (marked in orange color) coatings, at 9 weeks after surgery. \*\*\*\*\* Represents highly significant differences ( $p \leq 0.00001$ ).

## 5. Discussion

Because the biomaterials' osteoinduction mechanism is not yet entirely understood, one could not precisely answer the question whether if the sole biomaterial or an interaction between the biomaterial and the relevant proteins present in the living system are responsible for the osteoinduction process. Because most of the implants do not possess the capability to induce bone growth, specific material properties are required to activate the osteoinduction process. To begin the differentiation of the undifferentiated inducible osteoprogenitor cells into bone-forming cells, it was suggested that both the chemistry and the geometry of the biomaterial in contact with these cells represent critical factors to be considered [119].

Metallic implants (including Ti) are generally used for various biomedical applications, mainly due to their resistance to corrosion and favorable mechanical characteristics [120]. Because of its bioinert nature, bulk Ti is not capable to form a biochemical bond with the bone, and this biological inactivity often generates a fibrous tissue that surrounds the implanted device [121]. To improve both osseointegration rates and longevity of Ti implants, the deposition of CaP-based coatings onto their surfaces is envisaged. It was therefore demonstrated that implants' surface functionalization with CaP-based coatings could promote the formation of real bonds with the surrounding bone, due to their proved chemical similarity with natural bone tissue and their high biocompatibility [122]. This process occurs rapidly along the entire surface of the coating, in comparison to the case of simple Ti implants (used as controls in the experiments) [47].

A nowadays growing research interest in the field of biomaterials is related to the use of biological-derived CaP materials as viable, safe, and low-cost alternatives to synthetic CaP-ones [33]. It should be emphasized that, unfortunately, the Earth's available mineral resources are threatened to become limited in the near future because of the rapid demographic increase and economic growth. The access to sustainable resources is therefore critical. Consequently, this will generate a beneficial economic and environmental impact over the society, allowing for an intelligent use of these renewable resources.

The mechanical properties of CaP-based coatings are responsible with the overall success rate of an implant [123]. Thus, the optimal functioning of an endosseous implant is directly influenced by the biomaterial's mechanical stability, which can be easily evaluated by extraction tests. To obtain information on the force that occurs between the bone tissue and implanted materials, various experimental study models have been developed, each of them with their own particularities [115,124,125]. In this respect, the investigation of the coating bond strength is typically performed by scratch [126–128], pull-off [129], tensile adhesion [130–132], or shear strength tests [133], respectively. It is important to emphasize upon that the ISO 13779-2:2008 standard requirement for tensile adhesion strength of CaP-based coatings, used for load-bearing applications, is of 15 MPa [134]. It was reported that, in general, CaP-based coatings synthesized by the PLD technique easily surpass this imposed value [33,59,135]. There are some studies in the literature concentrated on tensile strength measurements [136,137], which, very importantly, can provide a direct measurement of the attachment between the bone and the implant surface, being therefore influenced only by the chemical bonding between those two [138–140]. This way, the effects of friction and of mechanical forces introduced by surface roughness can be minimized [141]. In the case of animal trials, the implant's increased bone retention is considered a clinically relevant indicator of improved stability and capacity of the implants to carry loads without detaching. Unfortunately, this type of information cannot be acquired by histological or SEM investigations, which provide only limited information on the functional performance of an implant. One should note that in none of the studies included in this review, related to mechanical testing of CaP-based coatings, alteration or disruption of the implants were present. In general, the inferred values for all functionalized Ti implants demonstrated significantly improved bone attachment in comparison to Ti ones. Next to the PLD surface functionalization of metallic implants, a longer implantation time period was demonstrated to induce a positive influence on the overall bone bonding strength characteristics of the investigated medical devices. One should note that the fabrication by PLD of novel BioHA implant coatings derived from sustainable and inexpensive CaP-based resources, with improved mechanical properties, correlated with an increased bone fixation in vivo, could stand for a pioneering contribution to the progress of advanced medical devices.

In general, the results of the studies included in this review, obtained using standardized radiography and microradiography [63], computed tomography [72,73,75], histomorphometry [65–67,69], and tomodensitometry [71], have confirmed the osseointegration process (pointing to an increase in the osseous density), along with a strong bone–implant connection and no inflammatory process of the soft tissues. The histological investigations, performed with various microscopy techniques [32,52,63–65,67,70,72–75], have indicated

also new active bone formation and demonstrated no adverse inflammatory reactions or gaps around the sites of implantation or at the bone–implant interface, for any of the investigated structures. In addition, the bone and the implant were shown to tightly adhere to each other along the full length of the interface. One interesting observation was that the temperature applied during the deposition process seemed to play an important role in the bone growth of the synthesized structures, the osteoblasts in the newly formed bone tissue being shown clear and homogenous [52]. Moreover, the osteointegration rate was demonstrated to be slightly superior in the case of annealed samples, rather than for the non-annealed ones [64]. It seemed also that no matter what the laser source used (i.e., KrF or CO<sub>2</sub>), between the synthesized coatings, no significant statistical differences in the osteogenesis process were inferred [64]. Significantly higher values of the bone area between the implant surface and the boundaries and bone adherence ratios were inferred at various implantation time periods in the case of functionalized implants in comparison to control ones [73,75]. In this respect, in the case of control samples, a fibrous connective tissue between the metallic implants and the newly formed bone was shown, while in the case of the synthesized coatings, this layer could be observed only seldom [63].

Even though it is generally accepted that CaP-based coatings deposited by PLD improve bone strength and the initial osseointegration rate, the coatings' properties necessary to achieve an optimum bone response are yet to be determined. This is mainly because of the limited number of *in vivo* studies available in the dedicated literature. It should be emphasized upon that the *in vivo* testing should demonstrate stability in biological environment for up to 1 month, which corresponds to the initial healing phase of the implants [142]. The limitations on such experiments can be related to (i) the difficulty to select a suitable animal model in order to properly simulate the actual mechanical loading and unloading conditions in which an implant should function inside a living system; (ii) the need to sacrifice a large number of animals to reach a significant statistical relevance, able to validate the obtained results; (iii) the demands for high costs and long time frame in the case of clinical trials; (iv) the lack of coordination among material scientists and biologists and thus an insufficient understanding of this interdisciplinary subject; and (v) the serious ethical concerns related to the used animals (including also the choice of their correct number), as they might be sometimes subjected to painful procedures or toxic exposures during the experimental trials [143].

Taking into consideration all these aspects, a future important progress of CaP-based materials might be linked to a shift of the focus from osteoconduction to osteoinduction, e.g., by additive manufacturing of scaffolds with complex, controlled three-dimensional porous structures and development of novel ion-substituted CaPs with increased biological activity. Moreover, new strategies, possibly based on self-assembling and/or nanofabrication might be developed for the successful fabrication of load-bearing bone graft substitutes. In the future, the composition, microstructure, and molecular surface chemistry of various types of CaPs might be tailored in such a way to match the specific biological and metabolic requirements of tissues or disease states. The multilayer composite coating systems, fabricated by the PLD technique, should represent also a future trend, able to provide multifunctional properties for the biomedical implants.

## 6. Conclusions

This review summarizes a two decades achievements reported in the field of *in vivo* assessment of calcium phosphate (CaP)-based coatings deposited onto metallic implants by one of the most frequently used plasma-assisted techniques, i.e., pulsed laser deposition (PLD). Due to their proven biocompatibility, mechanical (high adherence), and osseointegration and osteoconduction properties, CaP-based bioceramics are widely used in the field of bone regeneration, both in orthopedics and dentistry. For an in-depth *in vivo* assessment of various CaP-based coatings synthesized by the PLD method only, the results of the studies included in this review were obtained using a wide range of investigation techniques, among which a special focus was put on standardized and (micro) radiographies, (micro)

computed tomography and histomorphometry, tomodensitometry, histology, scanning and transmission electron microscopies, and mechanical testing. It is important to note that all these results indicate superior osseointegration characteristics of the metallic (generally Ti) implants functionalized with CaP-based coatings when compared to simple (uncoated) Ti ones, which are considered as the “gold standard” for implantological applications.

In the last two decades, research studies performed on CaP-coated metallic implants by PLD resulted in an interesting progress in vitro and in vivo, while not enough comparable clinical results were delivered so far for an easier assessment. This was mainly because of the lack of standardization of the coating properties and in vivo models. Therefore, additional testing is still needed in this direction, both to be able to advance a certain “recipe” to obtain optimum in vivo results, and to further reveal the relative influence of implant design, surgical procedure, and coating characteristics (thickness, structure, porosity, and surface morphology, which includes the wettability behavior), on either short-term or long-term clinical beneficial effects of the CaP-based coatings. In addition, one should emphasize upon the growing interest on the biological-derived CaP-materials as viable, safe, and cheap alternatives to the CaP synthetic ones, along with their improved biological properties and a greater resemblance to the mineral part of the human bones. The domain of PLD synthesis of natural-CaP sustainable coatings is in its first stages of development, and therefore, various possibilities to expand in the near future in terms of natural-CaP new resources, different concentrations of doping agents, or morphology and structural control of the obtained coatings are envisaged.

**Funding:** L.D. acknowledges the financial support of the Romanian Ministry of Education and Research under Romanian National Nucleu Program LAPLAS VI—contract No. 16N/2019.

**Institutional Review Board Statement:** The animal surgical protocols complied with the regulations and precautions of ISO-10993-Part 2 and Part 6, National Animal Care Guidelines and EU Council Directive of 22 September 2010, regarding the care and use of laboratory animals for scientific purposes (2010/63/EU), and were approved by the Institutional Animal-Care Committee, the Local Ethical Committee for the Affairs of Experiments on Animals in Lodz (22.12.2008, decree No. 56/ŁB 440/2008), the Osaka Dental University Ethics Committee, Japan (approval No. 16-08002, 2 August 2016), and the “Committee of Ethics and Academic and Scientific Deontology” at the UMF in Craiova, Romania (document No. 135/20.12.2019).

**Informed Consent Statement:** Informed consent was obtained from all subjects involved in the study.

**Data Availability Statement:** The data presented in this review are available in Refs. [32,52,63–75].

**Acknowledgments:** L.D. acknowledges F.N. Oktar (Marmara University, Istanbul) for providing animal-origin powders that were used for a part of the studies reported in this review. L.D. thanks George E. Stan for his useful comments and kind help.

**Conflicts of Interest:** The author declares no conflict of interest.

## References

1. Surmenev, R.A.; Surmeneva, M.A.; Ivanova, A.A. Significance of calcium phosphate coatings for the enhancement of new bone osteogenesis—A review. *Acta Biomater.* **2014**, *2*, 557–579. [CrossRef] [PubMed]
2. Allied Market Research. Available online: <https://www.alliedmarketresearch.com/implantable-medical-devices-market> (accessed on 10 December 2020).
3. Eliaz, N.; Metoki, N. Calcium Phosphate Bioceramics: A Review of Their History, Structure, Properties, Coating Technologies and Biomedical Applications. *Materials* **2017**, *10*, 334. [CrossRef] [PubMed]
4. Oladele, I.O.; Agbabiaka, O.; Olasunkanmi, O.G.; Balogun, A.O.; Popoola, M.O. Non-synthetic sources for the development of hydroxyapatite. *J. Appl. Biotechnol. Bioeng.* **2018**, *5*, 88–95. [CrossRef]
5. Akram, M.; Ahmed, R.; Shakir, I.; Ibrahim, W.A.W.; Hussain, R. Extracting hydroxyapatite and its precursors from natural resources. *J. Mater. Sci.* **2014**, *49*, 1461–1475. [CrossRef]
6. Šupová, M. Substituted hydroxyapatites for biomedical applications: A review. *Ceram. Int.* **2015**, *41*, 9203–9231. [CrossRef]
7. Graziani, G.; Boi, M.; Bianchi, M. A Review on Ionic Substitutions in Hydroxyapatite Thin Films: Towards Complete Biomimeticism. *Coatings* **2018**, *8*, 269. [CrossRef]

8. Tite, T.; Popa, A.C.; Balescu, L.M.; Bogdan, I.M.; Pasuk, I.; Ferreira, J.M.F.; Stan, G.E. Cationic substitutions in hydroxyapatite: Current status of the derived biofunctional effects and their in vitro interrogation methods. *Materials* **2018**, *11*, 2081. [[CrossRef](#)]
9. Ballini, A.; Mastrangelo, F.; Gastaldi, G.; Tettamanti, L.; Bukvic, N.; Cantore, S.; Cocco, T.; Saini, R.; Desiate, A.; Gherlone, E.; et al. Osteogenic differentiation and gene expression of dental pulp stem cells under low-level laser irradiation: A good promise for tissue engineering. *J. Biol. Regul. Homeost. Agents* **2015**, *29*, 813–822.
10. Barrere, F.; van der Valk, C.M.; Meijer, G.; Dalmeijer, R.A.; Groot, K.; Layrolle, P. Osteointegration of biomimetic apatite coating applied onto dense and porous metal implants in femurs of goats. *J. Biomed. Mater. Res. B Appl. Biomater.* **2003**, *67*, 655–665. [[CrossRef](#)]
11. Surmenev, R.A.; Surmeneva, M.A. A critical review of decades of research on calcium phosphate-based coatings: How far are we from their widespread clinical application? *Curr. Opin. Biomed. Eng.* **2019**, *10*, 35–44. [[CrossRef](#)]
12. Dorozhkin, S.V. Biphasic, triphasic, and multiphasic calcium orthophosphates. In *Advanced Ceramic Materials*; Tiwari, A., Gerhardt, R.A., Szutkowska, M., Eds.; Wiley, Scrivener Publishing: Austin, TX, USA, 2016; pp. 33–95.
13. Kang, Z.; Zhang, J.; Niu, L. A one-step hydrothermal process to fabricate superhydrophobic hydroxyapatite coatings and determination of their properties. *Surf. Coat. Technol.* **2018**, *334*, 84–89. [[CrossRef](#)]
14. Ciobanu, C.S.; Popa, C.L.; Predoi, D. Cerium-doped hydroxyapatite nanoparticles synthesized by the co-precipitation method. *J. Serb. Chem. Soc.* **2016**, *81*, 433–446. [[CrossRef](#)]
15. Raucci, M.G.; Demetri, C.; Soriente, A.; Fasolino, I.; Sannino, A.; Ambrosio, L. Gelatin/nano-hydroxyapatite hydrogel scaffold prepared by sol-gel technology as filler to repair bone defects. *J. Biomed. Mater. Res. Part A* **2018**, *106*, 2007–2019. [[CrossRef](#)] [[PubMed](#)]
16. Guoqing, M. Three common preparation methods of hydroxyapatite. *IOP Conf. Ser. Mater. Sci. Eng.* **2019**, *688*, 033057. [[CrossRef](#)]
17. Hare'l, G.; Ravi, B.G.; Chaim, R. Effects of solvent and agitation on microstructural characteristics of sol-gel derived nanocrystalline Y-TZP powders. *Mater. Lett.* **1999**, *39*, 63–68. [[CrossRef](#)]
18. Eshtiagh-Hosseini, H.; Housaindokht, M.R.; Chahkandi, M. Effects of parameters of sol-gel process on the phase evolution of sol-gel-derived hydroxyapatite. *Mater. Chem. Phys.* **2007**, *106*, 310–316.
19. Rey, C.; Combes, C.; Drouet, C.; Glimcher, M.J. Bone mineral: Update on chemical composition and structure. *Osteoporos. Int.* **2009**, *20*, 1013–1021. [[CrossRef](#)]
20. Niakan, A.; Ramesh, S.; Ganesan, P.; Tan, C.Y.; Purbolaksono, J.; Chandran, H.; Teng, W.D. Sintering behaviour of natural porous hydroxyapatite derived from bovine bone. *Ceram. Int.* **2015**, *41*, 3024–3029. [[CrossRef](#)]
21. Ofudje, E.A.; Rajendran, A.; Adeogun, A.I.; Idowu, M.A.; Kareem, S.O.; Pattanayak, D.K. Synthesis of organic derived hydroxyapatite scaffold from pig bone waste for tissue engineering applications. *Adv. Powder Technol.* **2018**, *29*, 1–8. [[CrossRef](#)]
22. Panda, N.N.; Pramanik, K.; Sukla, L.B. Extraction and characterization of biocompatible hydroxyapatite from fresh water fish scales for tissue engineering scaffold. *Bioprocess Biosyst. Eng.* **2014**, *37*, 433–440. [[CrossRef](#)]
23. Boutinguiza, M.; Pou, J.; Comesaña, R.; Lusquiños, F.; de Carlos, A.; León, B. Biological hydroxyapatite obtained from fish bones. *Mater. Sci. Eng. C Mater. Biol. Appl.* **2012**, *32*, 478–486. [[CrossRef](#)]
24. Iriarte-Velasco, U.; Sierra, I.; Zudaire, L.; Ayastuy, J.L. Conversion of waste animal bones into porous hydroxyapatite by alkaline treatment: Effect of the impregnation ratio and investigation of the activation mechanism. *J. Mater. Sci.* **2015**, *50*, 7568–7582. [[CrossRef](#)]
25. Shavandi, A.; El-Din, A.; Bekhit, A.; Ali, A.; Sun, Z. Synthesis of nano-hydroxyapatite (nHA) from waste mussel shells using a rapid microwave method. *Mater. Chem. Phys.* **2015**, *149–150*, 607–616. [[CrossRef](#)]
26. Tãmãsan, M.; Ozyegin, L.S.; Oktar, F.N.; Simon, V. Characterization of calcium phosphate powders originating from *Phyllacanthus imperialis* and *Trochidae Infundibulum concavus* marine shells. *Mater. Sci. Eng. C* **2013**, *33*, 2569–2577. [[CrossRef](#)] [[PubMed](#)]
27. Terzioğlu, P.; Ögütçü, H.; Kalemtaş, A. Natural calcium phosphates from fish bones and their potential biomedical applications. *Mater. Sci. Eng. C* **2018**, *91*, 899–911. [[CrossRef](#)] [[PubMed](#)]
28. Herliansyah, M.K.; Hamdi, M.; Ide-Ektessabi, A.; Wildan, M.W.; Toque, J.A. The influence of sintering temperature on the properties of compacted bovine hydroxyapatite. *Mater. Sci. Eng. C* **2009**, *29*, 1674–1680. [[CrossRef](#)]
29. Pietak, A.M.; Reid, J.W.; Stott, M.J.; Sayer, M. Silicon substitution in the calcium phosphate bioceramics. *Biomaterials* **2007**, *28*, 4023–4032. [[CrossRef](#)]
30. Hoyer, B.; Bernhardt, A.; Heinemann, S.; Stachel, I.; Meyer, M.; Gelinsky, M. Biomimetically Mineralized Salmon Collagen Scaffolds for Application in Bone Tissue Engineering. *Biomacromolecules* **2012**, *13*, 1059–1066. [[CrossRef](#)]
31. Rincón-López, J.A.; Hermann-Muñoz, J.A.; Giraldo-Betancur, A.L.; De Vizcaya-Ruiz, A.; Alvarado-Orozco, J.M.; Muñoz-Saldaña, J. Synthesis, characterization and in vitro study of synthetic and bovine-derived hydroxyapatite ceramics: A comparison. *Materials* **2018**, *11*, 333. [[CrossRef](#)]
32. Hayami, T.; Hontsu, S.; Higuchi, Y.; Nishikawa, H.; Kusunoki, M. Osteoconduction of a stoichiometric and bovine hydroxyapatite bilayer-coated implant. *Clin. Oral Implants Res.* **2011**, *22*, 774–776. [[CrossRef](#)]
33. Duta, L.; Popescu, A.C. Current Status on Pulsed Laser Deposition of Coatings from Animal-Origin Calcium Phosphate Sources. *Coatings* **2019**, *9*, 335. [[CrossRef](#)]
34. León, B.; John, J. *Thin Calcium Phosphate Coatings for Medical Implants*; Springer: New York, NY, USA, 2009; pp. 1–328.
35. Ambard, A.J.; Mueninghoff, L. Calcium phosphate cement: Review of mechanical and biological properties. *J. Prosthodont.* **2006**, *15*, 321–328. [[CrossRef](#)] [[PubMed](#)]

36. Sima, L.E.; Stan, G.E.; Morosanu, C.O.; Melinescu, A.; Ianculescu, A.; Melinte, R.; Neamtu, J.; Petrescu, S.M. Differentiation of mesenchymal stem cells onto highly adherent radio frequency-sputtered carbonated hydroxylapatite thin films. *J. Biomed. Mater. Res.* **2010**, *95*, 1203–1214. [[CrossRef](#)] [[PubMed](#)]
37. Popa, A.C.; Stan, G.E.; Besleaga, C.; Ion, L.; Maraloiu, V.A.; Tulyaganov, D.U.; Ferreira, J.M.F. Submicrometer Hollow Bioglass Cones Deposited by Radio Frequency Magnetron Sputtering: Formation Mechanism, Properties, and Prospective Biomedical Applications. *ACS Appl. Mater. Interfaces* **2016**, *8*, 4357–4367. [[CrossRef](#)] [[PubMed](#)]
38. Stan, G.E.; Popescu, A.C.; Mihailescu, I.N.; Marcov, D.A.; Mustata, R.C.; Sima, L.E.; Petrescu, S.M.; Ianculescu, A.; Trusca, R.; Morosanu, C.O. On the bioactivity of adherent bioglass thin films synthesized by magnetron sputtering techniques. *Thin Solid Films* **2010**, *518*, 5955–5964. [[CrossRef](#)]
39. Stan, G.E.; Marcov, D.A.; Pasuk, I.; Miculescu, F.; Pina, S.; Tulyaganov, D.U.; Ferreira, J.M.F. Bioactive glass thin films deposited by magnetron sputtering technique: The role of working pressure. *Appl. Surf. Sci.* **2010**, *256*, 7102–7110. [[CrossRef](#)]
40. Chrisey, D.B.; Hubler, G.K. (Eds.) *Pulsed Laser Deposition of Thin Films*, 1st ed.; John Wiley & Sons: Hoboken, NJ, USA, 1994; pp. 1–649.
41. Eason, R. *Pulsed Laser Deposition of Thin Films—Applications—Led Growth of Functional Materials*; Wiley-Interscience: Hoboken, NJ, USA, 2006; pp. 1–682.
42. Bao, Q.; Chen, C.; Wang, D.; Ji, Q.; Lei, T. Pulsed laser deposition and its current research status in preparing hydroxyapatite thin films. *Appl. Surf. Sci.* **2005**, *252*, 1538–1544. [[CrossRef](#)]
43. Rath, M.; Varadarajan, E.; Natarajan, V.; Rao, M.S.R. A comparative study on macroscopic and nanoscale polarization mapping on large area PLD grown PZT thin films. *Ceram. Int.* **2018**, *44*, 8749–8755. [[CrossRef](#)]
44. Cheang, P.; Khor, K.A. Addressing processing problems associated with plasma spraying of hydroxyapatite coatings. *Biomaterials* **1996**, *17*, 537–544. [[CrossRef](#)]
45. Epinette, J.A.; Manley, M.T. *Fifteen Years of Clinical Experience with Hydroxyapatite Coatings in Joint Arthroplasty*, 1st ed.; Springer: Paris, France, 2004; p. 452. [[CrossRef](#)]
46. Bose, S.; Tarafder, S.; Bandyopadhyay, A. Hydroxyapatite coatings for metallic implants. In *Hydroxyapatite (Hap) for Biomedical Applications*; Mucalo, M., Ed.; Woodhead Publishing Series in Biomaterials; Elsevier: Amsterdam, The Netherlands, 2015; pp. 143–157.
47. Yingchao, S.; Irsalan, C.; Yufeng, Z.; Liping, T.; Yi-Xian, Q.; Donghui, Z. Biofunctionalization of metallic implants by calcium phosphate coatings. *Bioact. Mat.* **2019**, *4*, 196–206. [[CrossRef](#)]
48. Yoshinari, M.; Hayakawa, T.; Wolke, J.G.; Nemoto, K.; Jansen, J.A. Influence of rapid heating with infrared radiation on RF magnetron-sputtered calcium phosphate coatings. *J. Biomed. Mater. Res.* **1997**, *37*, 60–67. [[CrossRef](#)]
49. Surmenev, R.A. A review of plasma-assisted methods for calcium phosphate-based coatings fabrication. *Surf. Coat. Technol.* **2012**, *206*, 2035–2056. [[CrossRef](#)]
50. Duta, L.; Oktar, F.N.; Stan, G.E.; Popescu-Pelin, G.; Serban, N.; Luculescu, C.; Mihailescu, I.N. Novel doped hydroxyapatite thin films obtained by pulsed laser deposition. *Appl. Surf. Sci.* **2013**, *265*, 41–49. [[CrossRef](#)]
51. Zeng, H. *Evaluation of Bioceramic Coatings Produced by Pulsed Laser Deposition and Ion Beam Sputtering*; University of Alabama at Birmingham: Birmingham, AL, USA, 1997.
52. Wang, D.G.; Chena, C.Z.; Ma, Q.S.; Jin, Q.P.; Li, H.C. A study on in vitro and in vivo bioactivity of HA/45S5 composite films by pulsed laser deposition. *Appl. Surf. Sci.* **2013**, *270*, 667–674. [[CrossRef](#)]
53. Schneider, C.W.; Lippert, T. Laser Ablation and Thin Film Deposition. In *Laser Processing of Materials*; Schaaf, P., Ed.; Springer Series in Materials Science; Springer: Berlin/Heidelberg, Germany, 2010; Volume 139, pp. 89–112.
54. Caricato, A.P.; Martino, M.; Romano, F.; Mirchin, N.; Peled, A. Pulsed laser photodeposition of a-Se nanofilms by ArF laser. *Appl. Surf. Sci.* **2007**, *253*, 6517–6521. [[CrossRef](#)]
55. Hashimoto, Y.; Ueda, M.; Kohiga, Y.; Imura, K.; Hontsu, S. Application of fluoridated hydroxyapatite thin film coatings using KrF pulsed laser deposition. *Dent. Mater. J.* **2018**, *37*, 408–413. [[CrossRef](#)]
56. Zaki, A.M.; Blythe, H.J.; Heald, S.M.; Fox, A.M.; Gehring, G.A. Growth of high quality yttrium iron garnet films using standard pulsed laser deposition technique. *J. Magn. Magn. Mater.* **2018**, *453*, 254–257. [[CrossRef](#)]
57. Novotný, M.; Vondráček, M.; Marešová, E.; Fitl, P.; Bulíř, J.; Pokorný, P.; Havlová, Š.; Abdellaoui, N.; Pereira, A.; Hubík, P.; et al. Optical and structural properties of ZnO:Eu thin films grown by pulsed laser deposition. *Appl. Surf. Sci.* **2019**, *476*, 271–275. [[CrossRef](#)]
58. Gyorgy, E.; Ristoscu, C.; Mihailescu, I.N. Role of laser pulse duration and gas pressure in deposition of AlN thin films. *J. Appl. Phys.* **2001**, *90*, 456. [[CrossRef](#)]
59. Zhang, Z.; Dunn, M.F.; Xiao, T.; Tomsia, A.P.; Saiz, E. Nanostructured Hydroxyapatite Coatings for Improved Adhesion and Corrosion Resistance for Medical Implants. *Mat. Res. Soc. Symp. Proc.* **2002**, *703*, 291–296. [[CrossRef](#)]
60. Jain, P.; Mandal, T.; Prakash, P.; Garg, A.; Balani, K. Electrophoretic deposition of nanocrystalline hydroxyapatite on Ti6Al4V/TiO2 substrate. *J. Coat. Technol. Res.* **2013**, *10*, 263–275. [[CrossRef](#)]
61. Wen, C.; Guan, S.; Peng, L.; Ren, C.; Wang, X.; Hu, Z. Characterization and degradation behavior of AZ31 alloy surface modified by bone-like hydroxyapatite for implant applications. *Appl. Surf. Sci.* **2009**, *255*, 6433–6438. [[CrossRef](#)]
62. Bakhsheshi-Rad, H.; Idris, M.; Abdul-Kadir, M. Synthesis and in vitro degradation evaluation of the nano-HA/MgF2 and DCPD/MgF2 composite coating on biodegradable Mg–Ca–Zn alloy. *Surf. Coat. Technol.* **2013**, *222*, 79–89. [[CrossRef](#)]

63. Dostálová, T.; Jelínek, M.; Himmlová, L.; Grivas, C. Laser-Deposited Hydroxyapatite Films on Dental Implants—Biological Evaluation in vivo. *Laser Phys.* **1998**, *8*, 182–186.
64. Antonov, E.N.; Bagratashvili, V.N.; Popov, V.K.; Sobol, E.N.; Howdle, S.M.; Joiner, C.; Parker, K.G.; Parker, T.L.; Doktorov, A.A.; Likhanov, V.B.; et al. Biocompatibility of laser-deposited hydroxyapatite coatings on titanium and polymer implant materials. *J. Biomed. Opt.* **1998**, *3*, 423–428. [[CrossRef](#)]
65. Dostálová, T.; Himmlová, L.; Jelínek, M.; Grivas, C. Osseointegration of loaded dental implant with KrF laser hydroxyapatite films on Ti6Al4V alloy by minipigs. *J. Biomed. Opt.* **2001**, *6*, 239–243. [[CrossRef](#)]
66. Kim, H.; Vohra, Y.K.; Louis, P.J.; Lacefield, W.R.; Lemons, J.E.; Camata, R.P. Biphasic and Preferentially Oriented Microcrystalline Calcium Phosphate Coatings: In-vitro and In-vivo Studies. *Key Eng. Mat.* **2005**, *284–286*, 207–210. [[CrossRef](#)]
67. Péraire, C.; Arias, J.L.; Bernal, D.; Pou, J.; Leon, B.; Arano, A.; Roth, W. Biological stability and osteoconductivity in rabbit tibia of pulsed laser deposited hydroxyapatite coatings. *J. Biomed. Mater. Res. Part A* **2006**, *77*, 370–379. [[CrossRef](#)]
68. Mihailescu, I.N.; Lamolle, S.; Socol, G.; Miroiu, F.; Roenold, H.J.; Bigi, A.; Mayer, I.; Cuisinier, F.; Lyngstadaas, S.P. In vivo tensile tests of biomimetic titanium implants pulsed laser coated with nanostructured Calcium Phosphate thin films. *Adv. Mater.-Rapid Commun.* **2008**, *2*, 337–341.
69. Paz, M.D.; Chiussi, S.; González, P.; Serra, J.; León, B.; Alava, J.I.; Güemes, I.; Sánchez-Margallo, F.M. Osseointegration of Calcium Phosphate Nanofilms on Titanium Alloy Implants. *Key Eng. Mater.* **2008**, *361–363*, 645–648. [[CrossRef](#)]
70. Hontsu, S.; Hashimoto, Y.; Yoshikawa, Y.; Kusunoki, M.; Nishikawa, H.; Ametani, A. Fabrication of Hydroxyl Apatite Coating Titanium Web Scaffold Using Pulsed Laser Deposition Method. *J. Hard. Tissue Biol.* **2012**, *21*, 181–188. [[CrossRef](#)]
71. Duta, L.; Stan, G.E.; Popescu, A.C.; Socol, G.; Miroiu, F.M.; Mihailescu, I.N.; Ianculescu, A.; Poata, I.; Chiriac, A. Hydroxyapatite thin films synthesized by Pulsed Laser Deposition onto titanium mesh implants for cranioplasty applications. In Proceedings of the ROMOPTO International Conference on Micro- to Nano-Photonics III, Bucharest, Romania, 3–6 September 2012; Volume 8882, p. 888208. [[CrossRef](#)]
72. Mroz, W.; Budner, B.; Syroka, R.; Niedzielski, K.; Golanski, G.; Slosarczyk, A.; Schwarze, D.; Douglas, T.E.L. In vivo implantation of porous titanium alloy implants coated with magnesium-doped octacalcium phosphate and hydroxyapatite thin films using pulsed laser deposition. *J. Biomed. Mater. Res. B Appl. Biomater.* **2015**, *103*, 151–158. [[CrossRef](#)]
73. Chen, L.; Komasa, S.; Hashimoto, Y.; Hontsu, S.; Okazaki, J. In Vitro and In Vivo Osteogenic Activity of Titanium Implants Coated by Pulsed Laser Deposition with a Thin Film of Fluoridated Hydroxyapatite. *Int. J. Mol. Sci.* **2018**, *19*, 1127. [[CrossRef](#)]
74. Wang, D.G.; Chen, C.Z.; Yang, X.X.; Ming, X.C.; Zhang, W.L. Effect of bioglass addition on the properties of HA/BG composite films fabricated by pulsed laser deposition. *Ceram. Int.* **2018**, *44*, 14528–14533. [[CrossRef](#)]
75. Duta, L.; Neamtu, J.; Melinte, R.P.; Zureigat, O.A.; Popescu-Pelin, G.; Chioibas, D.; Oktar, F.N.; Popescu, A.C. In Vivo Assessment of Bone Enhancement in the Case of 3D-Printed Implants Functionalized with Lithium-Doped Biological-Derived Hydroxyapatite Coatings: A Preliminary Study on Rabbits. *Coatings* **2020**, *10*, 992. [[CrossRef](#)]
76. Rosengren, A.; Danielsen, N.; Bjursten, L.M. Inflammatory reaction dependence on implant localization in rat soft tissue models. *Biomaterials* **1997**, *18*, 979–987. [[CrossRef](#)]
77. Black, J.; Hastings, G. *Handbook of Biomaterial Properties*; Springer: New York, NY, USA, 2013; p. 676.
78. Habibovic, P.; Kruij, M.C.; Juhl, M.V.; Clyens, S.; Martinetti, R.; Dolcini, L.; Theilgaard, N.; van Blitterswijk, C.A. Comparative in vivo study of six hydroxyapatite-based bone graft substitutes. *J. Orthop. Res.* **2008**, *26*, 1363–1370. [[CrossRef](#)]
79. Marini, E.; Ballanti, P.; Silvestrini, G.; Valdinucci, F.; Bonucci, E. The presence of different growth factors does not influence bone response to hydroxyapatite: Preliminary results. *J. Orthopaed. Traumatol.* **2004**, *5*, 34–43. [[CrossRef](#)]
80. Rabiee, S.; Moztaaradeh, F.; Solati-Hashjin, M. Synthesis and characterization of hydroxyapatite cement. *J. Mol. Struct.* **2010**, *969*, 172–175. [[CrossRef](#)]
81. Brånemark, P.I.; Hansson, B.O.; Adell, R.; Breine, U.; Lindström, J.; Hallén, O.; Ohman, A. Osseointegrated implants in the treatment of the edentulous jaw. Experience from a 10-year period. *Scand. J. Plast. Reconstr. Surg. Suppl.* **1977**, *16*, 1–132. [[PubMed](#)]
82. Choi, A.H.; Karacan, I.; Ben-Nissan, B. Surface modifications of titanium alloy using nanobioceramic-based coatings to improve osseointegration: A review. *Mater. Technol.* **2018**, *742–751*. [[CrossRef](#)]
83. Martin, J.Y.; Schwartz, Z.; Hummert, T.W.; Schraub, D.M.; Simpson, J.; Lankford, J., Jr.; Dean, D.D.; Cochran, D.L.; Boyan, B.D. Effect of titanium surface roughness on proliferation, differentiation, and protein synthesis of human osteoblast-like cells (MG63). *J. Biomed. Mater. Res. A* **1995**, *29*, 389–401. [[CrossRef](#)]
84. Rupp, F.; Gittens, R.A.; Scheideler, L.; Marmur, A.; Boyan, B.D.; Schwartz, Z.; Geis-Gerstorfer, J. A review on the wettability of dental implant surfaces I: Theoretical and experimental aspects. *Acta Biomater.* **2014**, *10*, 2894–2906. [[CrossRef](#)]
85. Gittens, R.A.; Scheideler, L.; Rupp, F.; Hyzy, S.L.; Geis-Gerstorfer, J.; Schwartz, Z.; Boyan, B.D. A review on the wettability of dental implant surfaces II: Biological and clinical aspects. *Acta Biomater.* **2014**, *10*, 2907–2918. [[CrossRef](#)]
86. Elias, C.N.; Oshida, Y.; Lima, J.H.; Muller, C.A. Relationship between surface properties (roughness, wettability and morphology) of titanium and dental implant removal torque. *J. Mech. Behav. Biomed. Mater.* **2008**, *1*, 234–242. [[CrossRef](#)]
87. Massaro, C.; Rotolo, P.; De Riccardis, F.; Milella, E.; Napoli, A.; Wieland, M.; Textor, M.; Spencer, N.D.; Brunette, D.M. Comparative investigation of the surface properties of commercial titanium dental implants. Part I: Chemical composition. *J. Mater. Sci. Mater. Med.* **2002**, *13*, 535–548. [[CrossRef](#)]
88. Lee, T.Q.; Danto, M.I.; Kim, W.C. Initial stability comparison of modular hip implants in synthetic femurs. *Orthopedics* **1998**, *21*, 885–888.

89. Wong, M.; Eulenberger, J.; Schenk, R.; Hunziker, E. Effect of surface topology on the osseointegration of implant materials in trabecular bone. *J. Biomed. Mater. Res.* **1995**, *29*, 1567–1575. [[CrossRef](#)]
90. Svehia, M.; Morberg, P.; Zicat, B.; Bruce, W.; Sonnabend, D.; Walsh, W.R. Morphometric and mechanical evaluation of titanium implant integration: Comparison of five surface structures. *J. Biomed. Mater. Res.* **2000**, *51*, 15–22. [[CrossRef](#)]
91. Lavenus, S.; Louarn, G.; Layrolle, P. Nanotechnology and Dental Implants. *Int. J. Biomater.* **2010**, *915327*, 9. [[CrossRef](#)]
92. Samavedi, S.; Whittington, A.R.; Goldstein, A.S. Calcium phosphate ceramics in bone tissue engineering: A review of properties and their influence on cell behavior. *Acta Biomater.* **2013**, *9*, 8037–8045. [[CrossRef](#)]
93. Szczeń, A.; Hołysz, L.; Chibowski, E. Synthesis of hydroxyapatite for biomedical applications. *Adv. Colloid Interface Sci.* **2017**, *249*, 321–330. [[CrossRef](#)]
94. Harun, W.S.W.; Asri, R.I.M.; Alias, J.; Zulkifli, F.H.; Kadirgama, K.; Ghani, S.A.C.; Shariffuddin, J.H.M. A comprehensive review of hydroxyapatite-based coatings adhesion on metallic biomaterials. *Ceram. Int.* **2018**, *44*, 1250–1268. [[CrossRef](#)]
95. Park, J.B.; Lakes, R.S. Metallic implant materials, Ch 5. In *Biomaterials. An introduction*; Park, J.B., Lakes, R.S., Eds.; Springer: New York, NY, USA, 2007; pp. 99–137. [[CrossRef](#)]
96. Niinomi, M.; Nakai, M.; Hieda, J. Development of new metallic alloys for biomedical applications. *Acta Biomater.* **2012**, *11*, 3888–3903. [[CrossRef](#)]
97. Zheng, Y.F.; Gu, X.N.; Witte, F. Biodegradable Metals. *Mater. Sci. Eng. R Rep.* **2014**, *77*, 1–34. [[CrossRef](#)]
98. Zhu, D.; Su, Y.; Young, M.L.; Ma, J.; Zheng, Y.; Tang, L. Biological responses and mechanisms of human bone marrow mesenchymal stem cells to Zn and Mg biomaterials. *ACS Appl. Mater. Interfaces* **2017**, *33*, 27453–27461. [[CrossRef](#)]
99. Coelho, P.G.; Granjeiro, J.M.; Romanos, G.E.; Suzuki, M.; Silva, N.R.F.; Cardaropoli, G.; Thompson, V.P.; Lemons, J.E. Basic research methods and current trends of dental implant surfaces. *J. Biomed. Mater. Res. Appl. Biomater.* **2009**, *88*, 579–596. [[CrossRef](#)]
100. Lu, Y.P.; Chen, Y.M.; Li, S.T.; Wang, J.H. Surface nanocrystallization of hydroxyapatite coating. *Acta Biomater.* **2008**, *4*, 1865–1872. [[CrossRef](#)]
101. Barradas, A.M.C.; Yuan, H.; van Blitterswijk, C.A.; Habibovic, P. Osteoinductive biomaterials: Current knowledge of properties, experimental models and biological mechanisms. *Eur. Cell Mater.* **2011**, *21*, 407–429. [[CrossRef](#)]
102. Cui, Q.; Dighe, A.S.; Irvine, J.N., Jr. Combined angiogenic and osteogenic factor delivery for bone regenerative engineering. *Curr. Pharm. Des.* **2013**, *19*, 3374–3383. [[CrossRef](#)] [[PubMed](#)]
103. Sarikaya, B.; Aydin, H.M. Collagen/beta-tricalcium phosphate based synthetic bone grafts via dehydrothermal processing. *BioMed Res. Int.* **2015**, *2015*, 576532. [[CrossRef](#)] [[PubMed](#)]
104. Ghanaati, S.; Barbeck, M.; Orth, C.; Willershausen, I.; Thimm, B.W.; Hoffmann, C.; Rasic, A.; Sader, R.A.; Unger, R.E.; Peters, F.; et al. Influence of  $\beta$ -tricalcium phosphate granule size and morphology on tissue reaction in vivo. *Acta Biomater.* **2010**, *6*, 4476–4487. [[CrossRef](#)]
105. Lakstein, D.; Kopelovitch, W.; Barkay, Z.; Bahaa, M.; Hendel, D.; Eliaz, N. Enhanced osseointegration of grit-blasted, NaOH-treated and electrochemically hydroxyapatite-coated Ti-6Al-4V implants in rabbits. *Acta Biomater.* **2009**, *5*, 2258–2269. [[CrossRef](#)]
106. He, F.; Ren, W.; Tian, X.; Liu, W.; Wu, S.; Chen, X. Comparative study on in vivo response of porous calcium carbonate composite ceramic and biphasic calcium phosphate ceramic. *Mater. Sci. Eng. C* **2016**, *64*, 117–123. [[CrossRef](#)]
107. Okuda, T.; Ioku, K.; Yonezawa, I.; Minagi, H.; Kawachi, G.; Gonda, Y.; Murayama, H.; Shibata, Y.; Minami, S.; Kamihira, S.; et al. The effect of the microstructure of beta-tricalcium phosphate on the metabolism of subsequently formed bone tissue. *Biomaterials* **2007**, *28*, 2612–2621. [[CrossRef](#)]
108. Sennerby, L.; Dasmah, A.; Larsson, B.; Iverhed, M. Bone tissue responses to surface-modified zirconia implants: A histomorphometric and removal torque study in the rabbit. *Clin. Implant Dent. Relat. Res.* **2005**, *7*, S13–S20. [[CrossRef](#)]
109. Susin, C.; Qahash, M.; Hall, J.; Sennerby, L.; Wikesjö, U.M. Histological and biomechanical evaluation of phosphorylcholine-coated titanium implants. *J. Clin. Periodontol.* **2008**, *35*, 270–275. [[CrossRef](#)]
110. Neyt, J.G.; Buckwalter, J.A.; Carroll, N.C. Use of animal models in musculoskeletal research. *Iowa Orthop. J.* **1998**, *18*, 118–123.
111. Gilsanz, V.; Roe, T.F.; Gibbens, D.T.; Schulz, E.E.; Carlson, M.E.; Gonzalez, O.; Boechat, M.I. Effect of sex steroids on peak bone density of growing rabbits. *Am. J. Physiol.* **1988**, *255*, E416–E421. [[CrossRef](#)]
112. Ferguson, J.C.; Tangl, S.; Barnewitz, D.; Genzel, A.; Heimel, P.; Hruschka, V.; Redl, H.; Nau, T. A large animal model for standardized testing of bone regeneration strategies. *BMC Vet. Res.* **2018**, *14*, 330. [[CrossRef](#)]
113. Kruyt, M.C.; de Bruijn, J.D.; Wilson, C.E.; Oner, F.C.; van Blitterswijk, C.A.; Verbout, A.J.; Dhert, W.J.A. Viable osteogenic cells are obligatory for tissue-engineered ectopic bone formation in goats. *Tissue Eng.* **2003**, *9*, 327–336. [[CrossRef](#)]
114. Cancedda, R.; Giannoni, P.; Mastrogiacomo, M. A tissue engineering approach to bone repair in large animal models and in clinical practice. *Biomaterials* **2007**, *28*, 4240–4250. [[CrossRef](#)]
115. Pearce, A.I.; Richards, R.G.; Milz, S.; Schneider, E.; Pearce, S.G. Animal models for implant biomaterial research in bone: A review. *Eur. Cells Mater.* **2007**, *13*, 1–10. [[CrossRef](#)]
116. Mostafa, A.A.; Zaazou, M.H.; Chow, L.C.; Mahmoud, A.A.; Zaki, D.Y.; Basha, M.; Abdel Hamid, M.A.; Khallaf, M.E.; Sharaf, N.F.; Hamdy, T.M. Injectable nano amorphous calcium phosphate based in situ gel systems for the treatment of periapical lesions. *Biomed. Mater.* **2015**, *10*, 065006. [[CrossRef](#)]
117. Habibovic, P.; Li, J.; van der Valk, C.M.; Meijer, G.; Layrolle, P.; van Blitterswijk, C.A.; de Groot, K. Biological performance of uncoated and octacalcium phosphate-coated Ti6Al4V. *Biomaterials* **2005**, *26*, 23–36. [[CrossRef](#)]

118. Inkson, B.J. Scanning electron microscopy (SEM) and transmission electron microscopy (TEM) for materials characterization, Chapter 2. In *Materials Characterization Using Nondestructive Evaluation (NDE) Methods*, 1st ed.; Hübschen, G., Altpeter, I., Tschuncky, R., Herrmann, H.G., Eds.; Elsevier: Amsterdam, The Netherlands, 2016; Volume 43, pp. 17–43. [CrossRef]
119. Fujibayashi, S.; Neo, M.; Kim, H.M.; Kokubo, T.; Nakamura, T. Osteoinduction of porous bioactive titanium metal. *Biomaterials* **2004**, *25*, 443–450. [CrossRef]
120. Yeo, I.-S.L. Modifications of dental implant surfaces at the micro and nano-level for enhanced osseointegration. *Materials* **2020**, *13*, 89. [CrossRef]
121. Katta, P.P.K.; Nalliyar, R. Corrosion resistance with self-healing behavior and biocompatibility of Ce incorporated niobium oxide coated 316L SS for orthopedic applications. *Surf. Coat. Technol.* **2019**, *375*, 715–726. [CrossRef]
122. Dorozhkin, S.V. Multiphasic calcium orthophosphate (CaPO<sub>4</sub>) bioceramics and their biomedical applications. *Ceram. Int.* **2016**, *42*, 6529–6554. [CrossRef]
123. Pichugin, V.F.; Surmenev, R.A.; Shesterikov, E.V.; Ryabtseva, M.A.; Eshenko, E.V.; Tverdokhlebov, S.I.; Prymak, O.; Epple, M. The preparation of calcium phosphate coatings on titanium and nickel-titanium by rf-magnetron-sputtered deposition: Composition, structure and micromechanical properties. *Surf. Coat. Technol.* **2008**, *202*, 3913–3920. [CrossRef]
124. Salou, L.; Hoornaert, A.; Louarn, G.; Layrolle, P. Enhanced osseointegration of titanium implants with nanostructured surfaces: An experimental study in rabbits. *Acta Biomater.* **2015**, *11*, 494–502. [CrossRef]
125. Sul, Y.-T.; Johansson, C.; Albrektsson, T. A novel in vivo method for quantifying the interfacial biochemical bond strength of bone implants. *J. R. Soc. Interface* **2009**, *7*, 81–90. [CrossRef]
126. Dinda, G.P.; Shin, J.; Mazumder, J. Pulsed laser deposition of hydroxyapatite thin films on Ti-6Al-4V: Effect of heat treatment on structure and properties. *Acta Biomater.* **2009**, *5*, 1821–1830. [CrossRef]
127. Łatka, L.; Pawłowski, L.; Chicot, D.; Pierlot, C.; Petit, F. Mechanical properties of suspension plasma sprayed hydroxyapatite coatings submitted to simulated body fluid. *Surf. Coat. Technol.* **2010**, *205*, 954–960. [CrossRef]
128. ISO 20502:2005(E). *Fine Ceramics (Advanced Ceramics, Advanced Technical Ceramics)—Determination of Adhesion of Ceramic Coatings by Scratch Testing*; ISO: Geneva, Switzerland, 2005; Available online: [www.iso.org](http://www.iso.org) (accessed on 11 December 2020).
129. Gadow, R.; Killinger, A.; Stiegler, N. Hydroxyapatite coatings for biomedical applications deposited by different thermal spray techniques. *Surf. Coat. Technol.* **2010**, *205*, 1157–1164. [CrossRef]
130. Yi, J.; Song, L.; Liu, X.; Xiao, Y.; Wu, Y.; Chen, J.; Wu, F.; Gu, Z. Hydroxyapatite Coatings Deposited by Liquid Precursor Plasma Spraying: Controlled Dense and Porous Microstructures and Osteoblastic Cell Responses. *Biofabrication* **2010**, *2*, 045003. [CrossRef]
131. Dey, A.; Mukhopadhyay, A.K.; Gangadharan, S.; Sinha, M.K.; Basu, D.; Bandyopadhyay, N.R. Nanoindentation study of microplasma sprayed hydroxyapatite coating. *Ceram. Int.* **2009**, *35*, 2295–2304. [CrossRef]
132. Singh, G.; Singh, S.; Prakash, S. Surface characterization of plasma sprayed pure and reinforced hydroxyapatite coating on Ti6Al4V alloy. *Surf. Coat. Technol.* **2011**, *205*, 4814–4820. [CrossRef]
133. Gomes, P.S.; Botelho, C.; Lopes, M.A.; Santos, J.D.; Fernandes, M.H. Evaluation of human osteoblastic cell response to plasma-sprayed silicon-substituted hydroxyapatite coatings over titanium substrates. *J. Biomed. Mater. Res. Appl. Biomater.* **2010**, *94B*, 337–346. [CrossRef]
134. ISO 13779-2:2008. Implants for Surgery—Hydroxyapatite—Part 2: Coatings of Hydroxyapatite. Available online: <http://www.iso.org/> (accessed on 11 December 2020).
135. Duta, L.; Mihailescu, N.; Popescu, A.C.; Luculescu, C.R.; Mihailescu, I.N.; Çetin, G.; Gunduz, O.; Oktar, F.N.; Popa, A.C.; Kuncser, A.; et al. Comparative physical, chemical and biological assessment of simple and titanium-doped ovine dentine-derived hydroxyapatite coatings fabricated by pulsed laser deposition. *Appl. Surf. Sci.* **2017**, *413*, 129–139. [CrossRef]
136. Edwards, J.T.; Brunski, J.B.; Higuchi, H.W. Mechanical and morphologic investigation of the tensile strength of a bone hydroxyapatite interface. *J. Biomed. Mater. Res.* **1997**, *36*, 454–468. [CrossRef]
137. Skripitz, R.; Aspenberg, P. Tensile bond between bone and titanium: A reappraisal of osseointegration. *Acta Orthop. Scand.* **1998**, *69*, 315–319. [CrossRef]
138. Shannon, F.J.; Cottrell, J.M.; Deng, X.-H.; Crowder, K.N.; Doty, S.B.; Avaltroni, M.J.; Warren, R.F.; Wright, T.M.; Schwartz, J. A novel surface treatment for porous metallic implants that improves the rate of bony ongrowth. *J. Biomed. Mater. Res. A* **2008**, *86*, 857–864. [CrossRef]
139. Schumacher, T.C.; Tushtev, K.; Wagner, U.; Becker, C.; Große Holthaus, M.; Hein, S.B.; Haack, J.; Engelhardt, C.H.M.; Khassawna, T.E.; Rezwan, K. A novel, hydroxyapatite-based screw-like device for anterior cruciate ligament (ACL) reconstructions. *Knee* **2017**, *24*, 933–939. [CrossRef]
140. Aparicio, C.; Padrós, A.; Gil, F.-J. In vivo evaluation of micro-rough and bioactive titanium dental implants using histometry and pull-out tests. *J. Mech. Behav. Biomed.* **2011**, *4*, 1672–1682. [CrossRef]
141. Nakamura, T.; Yamamuro, T.; Higashi, S.; Kokubo, T.; Itoo, S. A new glass-ceramic for bone replacement: Evaluation of its bonding to bone tissue. *J. Biomed. Mater. Res.* **1985**, *19*, 685–698. [CrossRef]
142. Pezeshki, P.; Lugowski, S.; Davies, J.E. Dissolution behavior of calcium phosphate nanocrystals deposited on titanium alloy surfaces. *J. Biomed. Mater. Res.* **2010**, *94A*, 660–666. [CrossRef]
143. Paital, S.R.; Dahotre, N.B. Calcium phosphate coatings for bio-implant applications: Materials, performance factors, and methodologies. *Mater. Sci. Eng.* **2009**, *R66*, 1–70. [CrossRef]